nature cancer

Article

https://doi.org/10.1038/s43018-023-00709-6

Repeated peripheral infusions of anti-EGFRvIII CAR T cells in combination with pembrolizumab show no efficacy in glioblastoma: a phase 1 trial

Received: 29 April 2023

Accepted: 13 December 2023

Published online: 12 January 2024

Check for updates

Stephen J. Bagley[1,25] ✉, Zev A. Binder[2,3,4,25], Lamia Lamrani[5,6,7,25], Eliana Marinari[8,9,10,11], Arati S. Desai[1], MacLean P. Nasrallah[4,12], Eileen Maloney[2], Steven Brem[2,4], Robert A. Lustig[13], Goldie Kurtz[13], Michelle Alonso-Basanta[13], Pierre-Emmanuel Bonté[6], Christel Goudot[6], Wilfrid Richer[6,14], Eliane Piaggio[6], Shawn Kothari[15], Lea Guyonnet[16], Coralie L. Guerin[16], Joshua J. Waterfall[14,17], Suyash Mohan[18], Wei-Ting Hwang[19], Oliver Y. Tang[4,20], Meghan Logun[2,3,4], Meghna Bhattacharyya[4,21], Kelly Markowitz[1], Devora Delman[1], Amy Marshall[3], E. John Wherry[7,22,23], Sebastian Amigorena[6], Gregory L. Beatty[1,4], Jennifer L. Brogdon[24], Elizabeth Hexner[1], Denis Migliorini[8,9,10,11], Cecile Alanio[5,6,7] ✉ & Donald M. O'Rourke[2,3,4]

We previously showed that chimeric antigen receptor (CAR) T-cell therapy targeting epidermal growth factor receptor variant III (EGFRvIII) produces upregulation of programmed death-ligand 1 (PD-L1) in the tumor microenvironment (TME). Here we conducted a phase 1 trial (NCT03726515) of CAR T-EGFRvIII cells administered concomitantly with the anti-PD1 (aPD1) monoclonal antibody pembrolizumab in patients with newly diagnosed, EGFRvIII$^+$ glioblastoma (GBM) ($n = 7$). The primary outcome was safety, and no dose-limiting toxicity was observed. Secondary outcomes included median progression-free survival (5.2 months; 90% confidence interval (CI), 2.9–6.0 months) and median overall survival (11.8 months; 90% CI, 9.2–14.2 months). In exploratory analyses, comparison of the TME in tumors harvested before versus after CAR + aPD1 administration demonstrated substantial evolution of the infiltrating myeloid and T cells, with more exhausted, regulatory, and interferon (IFN)-stimulated T cells at relapse. Our study suggests that the combination of CAR T cells and PD-1 inhibition in GBM is safe and biologically active but, given the lack of efficacy, also indicates a need to consider alternative strategies.

Chimeric antigen receptor (CAR) T-cell therapy has demonstrated remarkable efficacy in hematologic malignancies, but not solid tumors[1,2]. Challenges have included a paucity of unique tumor antigens, impaired CAR T-cell trafficking to tumor sites, tumor heterogeneity and antigen loss, and the immunosuppressive tumor microenvironment (TME)[3,4]. Each of these effects is epitomized by glioblastoma (GBM)[5], the most common malignant primary brain tumor in adults[6]. Despite aggressive standard treatment consisting of surgical resection,

A full list of affiliations appears at the end of the paper. ✉e-mail: sbagley@pennmedicine.upenn.edu; cecile.alanio@curie.fr

Table 1 | Patient characteristics

Patient	Age (y)	Sex	Extent of surgical resection (contrast-enhancing tumor)	ECOG PS	EGFRvIII expression	Other NGS results (disease-associated variants only)	Measurable enhancing tumor (≥ 1 cm x 1 cm) at time of CAR T-cell infusion 1	Steroid dosage, apheresis[a]	Steroid dosage, CAR T-cell infusion 1[a]	Steroid dosage, final CAR T-cell infusion[a]
1	59	F	Gross total resection	1	34.70%	EGFR amplification, EGFR p.A289V, STAG2 p.D819Leufs*53	Yes	0	0	0
2	56	M	Near total resection	0	0.03%	EGFR amplification, NF1 p.E1220*	No	0	0	0
4	76	M	Partial resection	1	0.46%	EGFR amplification, PIK3CB p.E1051K	Yes	2	2	2
5	63	M	Gross total resection	0	0.02%	EGFR amplification, PIK3CA p.C901F	Yes	0	0	0
6	74	M	Gross total resection	0	0.15%	EGFR amplification, NF1 R304*	No	0	0	0
7	76	M	Partial resection	1	0.32%	EGFR amplification, PTEN p.? c.634+5 G>A	Yes	0	0	0
8	62	F	Near total resection	0	56.60%	EGFR amplification, STAG2 p.Q211*	Yes	0	0	0

ECOG PS, Eastern Cooperative Oncology Group Performance Status; F, female; M, male. [a]Steroid dosage is reported in milligrams dexamethasone per day.

radiation and temozolomide[7], median overall survival (OS) remains 15–18 months[8].

Results from phase I clinical trials of CAR T cells targeting epidermal growth factor receptor variant III (EGFRvIII)[9], HER2 (ref. 10) or IL-13Rα2 (ref. 11), administered systemically or by direct delivery into the central nervous system, have demonstrated feasibility and safety in patients with GBM. However, other than case reports[12,13], efficacy has been underwhelming. We previously conducted a first-in-human trial in 10 patients with recurrent GBM (rGBM) treated with a single peripheral infusion of CAR T cells targeted against EGFRvIII[9], an EGFR variant resulting from the in-frame deletion of exons 2–7 that is present in 25–30% of all patients with GBM[14–16]. We observed no off-tumor toxicity or cytokine release syndrome (CRS) and found successful trafficking of CAR T-EGFRvIII cells to regions of active GBM, with reduction of target antigen in 5 of 7 patients with available pre- and post-infusion tumor tissue[9]. Notably, higher PD-1 expression in the CAR T-cell infusion product correlated with increased peripheral CAR T-cell engraftment and longer progression-free survival (PFS) in these patients[17]. However, immunohistochemical interrogation of paired pre- and post-treatment tumor specimens demonstrated marked compensatory upregulation of inhibitory molecules and regulatory T cells in the local TME following CAR T-cell therapy. Among these targets, the most actionable was programmed death-ligand 1 (PD-L1), which showed robustly increased expression in GBM tumor tissue following administration of CAR T-EGFRvIII cells[9].

We hypothesized a role for the PD-1/PD-L1 axis in limiting the activity of CAR T cells in the TME. To test this hypothesis, we conducted a phase 1 clinical trial of peripherally delivered EGFRvIII-targeted CAR T cells plus the PD-1 inhibitor pembrolizumab in adult patients with EGFRvIII$^+$ GBM (NCT03726515). The study was conducted in the de novo setting, as EGFRvIII expression is lost at the time of recurrence in ~50–60% of patients who are positive for EGFRvIII at initial diagnosis[14,18]. The study did not lead to detectable clinical activity. To better understand the mechanisms underlying the apparent lack of treatment efficacy, and to detect actionable items that can potentially be improved in future clinical trials, we performed in-depth ancillary analyses. Specifically, we examined CAR T-cell features in the infusion product, their expansion in the blood after administration, their entry into brain tumors and their impact on the TME locally by examining pre- versus post-treatment tumor samples from a subset of patients. Despite the apparent lack of clinical efficacy, we found evidence for a biological impact of the treatment on the TME, with a likely infiltration of the infusion product into the tumor, and increased activation of the myeloid and T-cell compartment. We also observed that the amount of interferon (IFN) signaling in T cells at time of disease progression positively correlated with subsequent OS. Together, our observations help characterize the mechanisms of action of CAR T-cell therapy upon administration to patients with brain tumors but, given the lack of efficacy, also indicate a need to consider alternative strategies.

Results

Clinical results

Seven patients were treated between 22 April 2019 and 29 June 2020 (Table 1). All patients had histopathologically confirmed GBM according to the revised World Health Organization 2021 classification[19] and had already undergone resection. Other key eligibility criteria included adequate performance status, no severe or uncontrolled autoimmune disease and tumor tissue negative for *MGMT* promoter methylation. All patients provided written informed consent. Patients were not compensated for participation. All patients completed a hypofractionated course of radiation (40 Gy delivered in 15 fractions). Three patients completed all planned cycles of treatment, consisting of three cycles of combined CAR T-EGFRvIII cells plus pembrolizumab therapy and a fourth cycle consisting of pembrolizumab monotherapy; one patient completed two cycles of combined therapy; and three patients completed only one cycle of combined therapy. CAR T-cell dose and characteristics are summarized in Table 2.

All patients underwent repeat surgery for radiographic progression after having received at least one cycle of CAR T cells and pembrolizumab (Fig. 1a,b). Specifically, three patients underwent surgery within 3 weeks following the first cycle of CAR T-EGFRvIII cells and pembrolizumab (7 days, 14 days and 18 days, respectively). In addition, one patient underwent surgery at 13 weeks after the second cycle of combination therapy, and three patients underwent surgery after the third/final cycle of combination therapy (9 weeks, 12 weeks and 25 weeks, respectively).

The combination of CAR T-EGFRvIII cells and pembrolizumab appeared to be well tolerated in this small cohort, and no dose-limiting toxicities (DLTs) were observed (DLT rate, 0%; 95% confidence interval (CI), 0–43%). Adverse events (AEs) are displayed in Table 3. There were no suspected cases of CRS or immune effector cell-associated neurotoxicity syndrome. One patient had a severe immune-related

Table 2 | CAR T doses

Patient	Cycle 1		Cycle 2		Cycle 3	
	CAR T-EGFRvIII (cells/dose)	CAR T-EGFRvIII % Transd.	CAR T-EGFRvIII (cells/dose)	CAR T-EGFRvIII % Transd.	CAR T-EGFRvIII (cells/dose)	CAR T-EGFRvIII % Transd.
1	2×10^8	24.8	2×10^8	24.8	2×10^8	24.8
2	2×10^8	16.1	2×10^8	16.1	2×10^8	16.1
4	2×10^8	29.4	N/A		N/A	
5	2×10^8	22.3	2×10^8	22.3	2×10^8	22.3
6	2×10^8	28	2×10^8	28	2×10^8	28
7	4.65×10^7	28.6	N/A		N/A	
8	2×10^8	31.1	N/A		N/A	

N/A, not applicable; Transd., transduced.

AE likely related to pembrolizumab. This patient received three cycles of combined CAR T cells plus pembrolizumab and a fourth additional cycle of pembrolizumab alone. Twelve weeks after the fourth cycle of pembrolizumab, the patient presented with severe nausea and was found to have acute liver injury (AST 1,209 U liter^{-1}, ALT 3,367 U liter^{-1}, total bilirubin 1.5 mg dl^{-1}) and acute kidney injury (creatinine 7.6 mg dl^{-1}, baseline 1.2 mg dl^{-1}). Alternative etiologies were excluded and the patient was treated with 1 g intravenous methylprednisolone per day for 5 days followed by prolonged corticosteroid taper. Liver and kidney function tests normalized rapidly. No other immune-related AE were observed.

Median PFS for the cohort was 5.2 months (90% CI, 2.9–6.0 months); median OS was 11.8 months (90 % CI, 9.2–14.2 months). A swimmer's plot demonstrating timing of receipt of study interventions, disease progression, and death, as well as Kaplan–Meier curves, is displayed in Fig. 1b–d. Peripheral blood CAR T-cell engraftment kinetics from this study are displayed in Fig. 2a alongside those from our prior trial of a single peripheral infusion of EGFRvIII-directed CAR T cells in rGBM (Fig. 2b)[9]. Despite up to three infusions of CAR T cells, peripheral engraftment peak levels were nearly a log lower than that observed for rGBM patients who had received a single dose of EGFRvIII CAR T cells[9]. Next-generation sequencing (NGS)-determined EGFRvIII levels in the pre- and post-CAR T-cell infusion tumor tissue highlighted a decrease in target antigen in six of seven patients (Fig. 2c). Infusion product PD-1 levels showed no difference between the two studies, suggesting the starting material was comparable (Fig. 2d). Despite this, a correlation between PD-1 expression in the infusion product and CAR T-cell engraftment, as seen in our first trial in rGBM[17], was not recapitulated in this study in the de novo setting (Fig. 2e).

Infusion product CAR T cells have comparable features across patients

The heterogeneity in the composition of infusion products can lead to differences in clinical outcome. For example, higher amounts of memory T cells in the infusion product have been identified as predictive of later efficacy in chronic lymphocytic leukemia[20]. To investigate this in our trial, we phenotyped the infusion products of six out of seven patients in the cohort using flow cytometry. Using biotinylated EGFRvIII to track EGFRvIII-targeted CAR T cells (Extended Data Fig. 1a), we detected 21% (range, 20.6–28.5%) CAR$^+$ T cells within the CD3$^+$ T cells contained in the infusion product (Extended Data Fig. 1b). These proportions were similar across patients and in accordance with manufacturing regulations; 75% (range, 53.1–92.96%) of the detected CAR T cells were CD4$^+$ (Extended Data Fig. 1c,d). To further identify the T-cell state of the CAR and non-CAR T cells contained in the infusion products, we developed a 30-marker Cytek panel containing markers for T-cell activation (HLADR, CD38 and CD25), proliferation (Ki67), differentiation (CD45RA and CD27) and exhaustion (PD-1, TOX, CTLA4, Tim3 and CD39) (Supplementary Table 1). We used this panel to characterize the infusion products of two patients (patient 1 (P1) and P4).

We found that the CD4$^+$ CAR T cells contained in the infusion products were mostly CD127$^+$ CD25$^{-/+}$ (Extended Data Fig. 1e) and FoxP3$^-$ (Extended Data Fig. 1f), indicating that they are conventional CD4$^+$ T cells. This interpretation was confirmed by single-cell RNA sequencing (scRNAseq) on the infusion products from the two donors where the CD4$^+$ T cells identified in the infusion products were expressing high levels of CD40LG, a canonical marker for conventional T cells, and low levels of Foxp3 (Extended Data Fig. 1g). Most of the CD4$^+$ CAR T cells contained in the infusion products of the two donors were CD45RA$^-$, KLRG1$^-$ and CCR7$^-$, and they expressed 63% and 38% of CD27 in P1 and P4, respectively (Extended Data Fig. 1h). We concluded that the majority of the CD4$^+$ CAR T cells contained in the infusion products of the two tested patients were therefore activated conventional effector CD4 T cells.

Similar to CD4$^+$ T cells, most of the CD8$^+$ CAR T cells contained in the infusion products of the two donors were CD45RA$^-$, KLRG1$^-$ and CCR7$^-$ and expressed 68% and 29% of CD27 in P1 and P4, respectively (Extended Data Fig. 1i). As such, these cells were identified as effector memory 1 and effector memory 2 cells[21]. CAR CD8$^+$ T cells contained in the infusion product had a similar phenotype, being CD45RA$^+$CCR7$^-$KLRG1$^-$CD27$^{+/-}$. In P1 and P4, both the CD8$^+$ CAR$^+$ and CAR$^-$ T cells were activated (HLADR$^+$CD38$^+$CD25$^+$), proliferating (Ki67$^+$) and expressed some markers of T-cell exhaustion (TOX, Tim3 and LAG3) (Extended Data Fig. 1j,k). Some CD8$^+$ CAR T cells also co-expressed other checkpoint inhibitors such as PD-1, CTLA4 and TIGIT, indicating a higher degree of T-cell exhaustion (Extended Data Fig. 1k). Together, these findings suggested that the CAR and non-CAR CD8$^+$ T cells present in the infusion products were activated effector T cells that underwent some degree of exhaustion, likely related to the manufacturing in vitro. The only detectable difference among the two patients was a lower amount of CD39-expressing cells within CD8$^+$ CAR T cells in P4 as compared to P1 (Extended Data Fig. 1k, middle panel). All the other markers were consistent between the two donors. Overall, we concluded that the infusion products are composed of ~20% CAR T cells that were activated and exhausted effectors. Further studies are needed to confirm these results given the small number of patients.

CAR T cells are detectable in one patient's tumor after the infusion

In the current trial, the infusion products were administered intravenously. To be efficient and mediate their effect, EGFRvIII CAR T cells contained in the infusion products had to migrate through the blood-brain barrier and reach the brain tumor. Whether this process is efficient and accompanied by infiltration of the non-CAR T cells also contained in the infusion products is unclear. We were able to address this question using the unique collection of tumors

https://doi.org/10.1038/s43018-023-00709-6

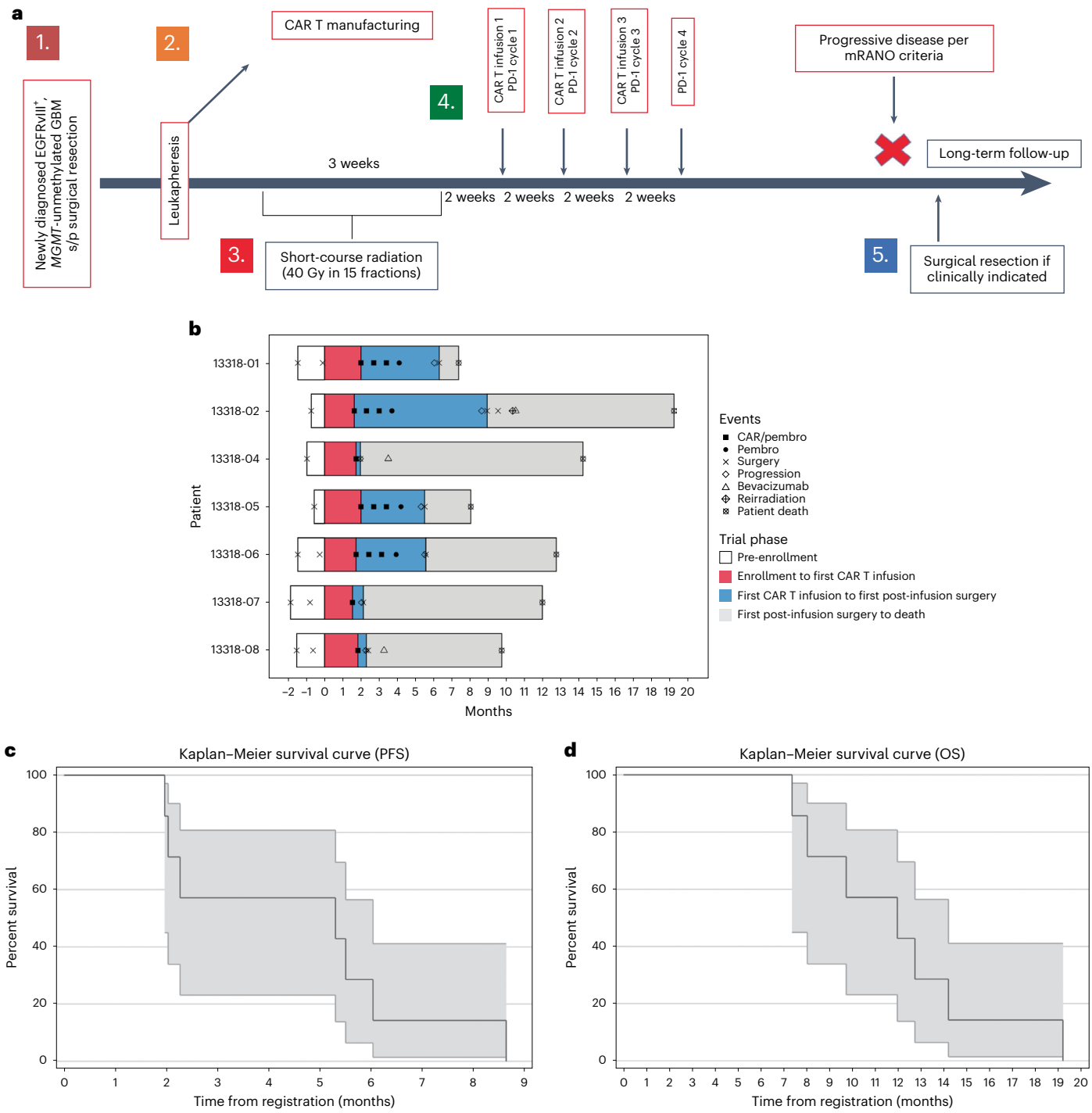

Fig. 1 | Study overview and outcomes. a, Study schema. mRANO, Modified Response Assessment in Neuro-Oncology; s/p, status post. **b**, Swimmer's plot displaying timing of CAR T-cell and pembrolizumab (pembro) infusions, surgical interventions, disease progression, post-study therapies and death for each patient ($n = 7$). **c**, Median PFS with 90% CI ($n = 7$). **d**, Median OS with 90% CI ($n = 7$).

obtained from patients before and after the infusion of CAR T cells (at the time of diagnosis and at the time of relapse after CAR T-cell therapy, respectively). Because the resection of tumors after CAR T-cell therapy was triggered by clinical indications, the delay from the last CAR T-cell infusion varied among patients, from 7 days (P4) to 179 days (P2) (Fig. 3a). At that time, using 4-1BB/CD3z (BBZ) quantitative polymerase chain reaction (qPCR), we could detect CAR T cells in the blood of five out of seven patients, with the highest amount in P4, who was reoperated on only 7 days after the last infusion of CAR T cells (Fig. 3b). In the brain, we could detect CAR T cells using BBZ qPCR in only one out of the seven tumors tested (Fig. 3c). The positive detection of CAR T cells in the brain tumor was for P4, the patient with the least amount of time between infusion of CAR T and acquisition of post-treatment tumor tissue (7 days). This patient also demonstrated the highest amount of CAR T cells in the peripheral circulation at this timepoint. These data suggest that infiltration of CAR T cells in tumors can occur at the peak of expansion in the blood. However, it was unclear whether the other patients also experienced an infiltration of CAR T cells in the tumor. Their absence at the time of progression could indicate a lack of either infiltration or persistence of the CAR T cells. To address this

https://doi.org/10.1038/s43018-023-00709-6

Table 3 | AEs with each patient counted once for a given toxicity at the highest grade observed

Common Terminology Criteria for Adverse Events category	Toxicity	Grade 1-2	Grade 3-4
Endocrine disorders	Hyperthyroidism	1	
Gastrointestinal disorders	Dysphagia	2	
	Nausea	1	
General disorders and administration site conditions	Breath odor–creamed corn	1	
	Fatigue	7	
	Fever	1	
	Gait disturbance	1	
Infections and infestations	Lung infection		1
Injury, poisoning and procedural complications	Fall	4	
Investigations	Dehydration	1	
	Hypertension	1	
	Lactic acidosis	1	
	Surgery fluid shifts	1	
Metabolism and nutrition disorders	Breath odor–creamed corn	1	
	Hyperglycemia	1	
	Hypernatremia	1	
Musculoskeletal and connective tissue disorders	Generalized muscle weakness	1	
	Muscle weakness, lower limb	1	
	Pain in extremity	2	
Nervous system disorders	Cerebral edema		1
	Cognitive disturbance	1	
	Dysphasia	1	
	Encephalopathy		1
	Facial muscle weakness	1	
	Headache	6	
	Muscle weakness, left-sided		1
	Seizure		1
Psychiatric disorders	Depression	1	
Skin and subcutaneous tissue disorders	Pruritus	1	
	Rash maculo-papular	5	
	Skin and subcutaneous tissue disorders–mild odor	1	
Vascular disorders	Hypertension	1	
	Thromboembolic event	1	

question, we performed scRNAseq and T-cell receptor sequencing (TCRseq) on the pre- and post-CAR T-cell paired tumor samples, which were available in three of the seven patients who had archival tumor tissue available from the original surgical resection at time of initial diagnosis (P1, P6 and P7), the post-CAR T-cell tumor samples available from the four remaining patients who did not have archival tumor tissue available from initial diagnosis (P2–P5), the blood of all patients at the time of the relapse, and the infusion products for two patients: P4, for whom we detected CAR T cells in the brain after infusion by qPCR, and P1, who was a longer survivor. We first established a bioinformatic pipeline to identify the CAR sequence among transcripts at the single-cell level (Extended Data Fig. 2a). Applying this pipeline to the scRNAseq data from the brain tumors, we found no CAR T cells for any of the patients. This included P4, despite previously detecting CAR T cells in the tumor via BBZ qPCR. The discrepancy observed between qPCR and scRNAseq results for P4 can be explained by the lower sensitivity of scRNAseq, which could not detect the low amount of CAR T cells detected by BBZ qPCR. However, when considering the clonotypes included in the infusion products and in the tumor and blood at the time of tumor progression, we found that the infusion product and the tumor after infusion shared some clones, and in a larger amount for P4 as compared to P1 (Fig. 3d,e and Extended Data Fig. 2b,c). Of interest, all of the clones that were shared between the infusion product and the tumor were also present in the blood. However, a few clones present in the blood were found in the tumor but not in the infusion product. Although we cannot rule out that the large sharing of T-cell receptors (TCRs) across the infusion product and the tumor reflect a sharing of blood TCRs, it is also possible that a substantial proportion of the non-CAR T cells contained in the infusion products penetrated the tumors. Taken together, these results suggest that the T cells in the infusion product penetrated the brain tumors after peripheral blood administration and that the infiltration of CAR T cells was likely accompanied by the entry of bystander non-CAR T cells both from the infusion product and from the blood. One potential hypothesis is that the CAR T cells penetrated the tumor at the peak of peripheral blood expansion but did not persist, potentially contributing to the lack of clinical efficacy observed in this trial. Further studies are warranted to confirm this hypothesis.

No major changes in overall immune composition of tumors with therapy

With infusion product penetration of the brain tumors, one of the goals was to have a positive impact on the immunosuppressive TME. To detect and characterize the impact of the CAR T-cell therapy plus pembrolizumab on the TME of GBM, we performed scRNAseq on paired tumor samples (before and after CAR T-cell infusion) for 3 patients (Patient 1, P1, Patient 6, P6, and Patient 7, P7; Fig. 4a). In order to detect changes in the immune populations, scRNAseq was performed on CD45-enriched cells after magnetic enrichment (Fig. 4b), which was favored over flow-based sorting because of limited starting material. The proportion of $CD45^+$ cells was 1.8% ± 2.9% before enrichment, and we obtained an average of 41.9% ± 23.4% $CD45^+$ cells after enrichment. These post-enrichment suspensions were loaded on the 10x Genomics chip for scRNAseq (Methods). Although this is a substantial enrichment, it is not 100% effective and allowed for non-hematopoietic cells to be loaded onto the 10x Genomics chip and analyzed with scRNAseq. We obtained a total of 11,424 cells over the 6 samples (Extended Data Fig. 2d,e). Overall, the TME was dominated by macrophages and T cells, together with fewer B cells, cycling cells, pericytes/stromal cells, endothelial cells, and some contaminating neoplastic cells (Fig. 4c,d). Of note, we found an average of 35% ± 23% T cells within CD45-enriched cells, which is substantially higher than in our previous report[22]. Although we cannot rule out that some circulating $CD45^+$ cells from the tumor vasculature may be included, we believe this to be a very minor fraction, as cell types such as naive T cells and monocytes, which are typically abundant in blood and not in tissue, were not identified in our analysis. Our interpretation is that this reflects a bias of the magnetic enrichment toward more T cells, as myeloid cells in GBM are often $CD45^{low}$, which makes them less easy to enrich with $CD45^+$ selection. When comparing pre- versus post-CAR T-cell therapy samples, we found that P1 had a detectable increase in T-cell proportions over time (Fig. 4e,f). Interestingly, P1 also expressed higher amounts of the target EGFRvIII (35%) and had a longer OS. Although not significant, we also detected a trend for increased proportions of tumor-associated macrophages in all three patients (Fig. 4f).

To better understand how myeloid cells were qualitatively impacted during the course of the therapy, we further separated the CD68, CD163 and/or CD14 expressing cells from the global Uniform

https://doi.org/10.1038/s43018-023-00709-6

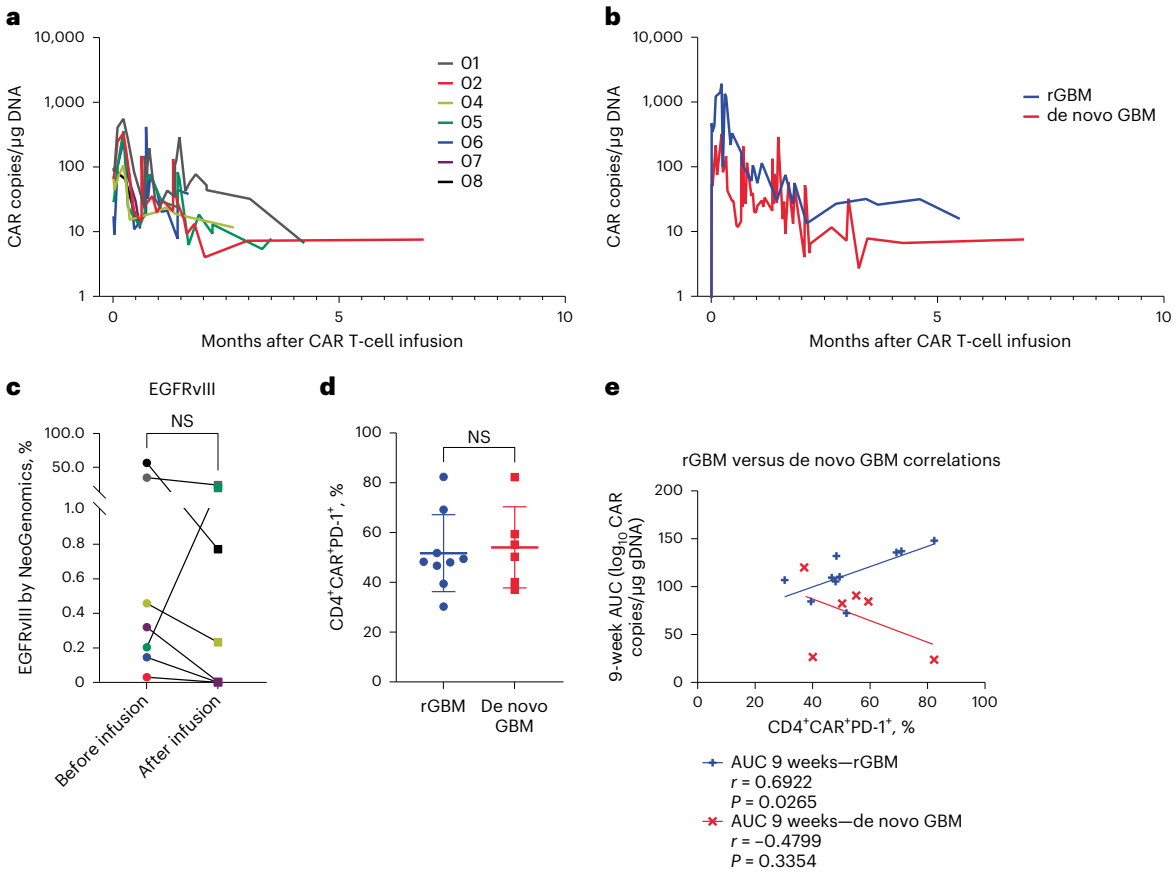

Fig. 2 | Peripheral blood CAR T-cell levels, target expression and infusion product characterization. a, Peripheral blood levels of CAR T cells for individual patients ($n = 7$). **b**, Average peripheral blood CAR T-cell levels from our current de novo GBM trial (NCT03726515, $n = 7$) compared to our prior rGBM trial (NCT02209376, $n = 10$). **c**, NGS EGFRvIII quantification in tumor tissue before and after CAR T-cell infusion in the de novo GBM trial ($n = 7$). **d**, PD-1 expression in the $CD4^+/CAR^+$ infusion product in the de novo ($n = 7$) versus rGBM ($n = 10$) trial (two-tailed unpaired *t*-test; data are presented as mean values ± standard error of the mean). **e**, PD-1 levels correlated to 9-week area under the curve (AUC) values in the de novo versus rGBM trial (two-tailed Pearson correlation). NS, not significant.

Manifold Approximation and Projection (UMAP) (Extended Data Fig. 3a). Based on the top genes expressed, we identified six clusters of myeloid cells as inflammatory macrophages, monocyte-derived macrophages, $TREM2^{hi}$ microglia, dendritic cells, IL-32+ myeloid cells and $BEST1^+$ myeloid cells (Extended Data Fig. 3a–f). When comparing pre- versus post-CAR T-cell therapy samples, we detected important interindividual variation, with decreased $TREM2^{hi}$ microglia cells and increased monocyte-derived macrophages in P1 only (Extended Data Fig. 3g).

Increased IFN-stimulated T cells correlates with outcomes

Despite comparable proportions of T cells in the TME before and after the treatment, it is possible that the changes observed in the myeloid compartment over the course of the treatment were accompanied by some changes in the state of the T cells present in the tumor. To gain more insight into more subtle changes in the T-cell compartment with the therapy, we subsetted cells that expressed CD3D, CD3E and/or CD247. Based on top genes expressed, we could identify five clusters of T cells and two clusters of natural killer cells (Fig. 5a). Clusters of T cells contained two clusters of CD4 T cells (conventional memory CD4 T cells and regulatory T cells), two clusters of CD8 T cells (resident memory CD8 T cells, and effector exhausted CD8 T cells) and one cluster of both CD4 and CD8 T cells that were IFN stimulated (Fig. 5b). When considering the gene expression before versus after CAR T-cell therapy, we noticed an increase of exhaustion markers after treatment (TOX, PDCD1, Eomes and Slamf6) (Fig. 5c). Despite important inter-individual variations, we also observed in all three patients an increase in IFN-stimulated T cells (ratio paired *t*-test $P = 0.02$) over the course of the treatment (Fig. 5d,e). Gene set enrichment analysis (GSEA) revealed that the IFN-stimulated signature was composed of both IFN-gamma- and alpha-related genes (Fig. 5f). When using the IFN signature to map onto the seven patients of the cohort at the time of tumor progression, we found that the intensity of the IFN-related signature in T cells was positively correlated to time from tumor progression to death (spearman $P = 0.03$, Fig. 5g,h). Together, our data demonstrate an increase in inflammation in the T-cell compartment following treatment that was associated with clinical outcomes. Further studies are needed to determine the extent to which these changes were driven by CAR T cells plus pembrolizumab versus the natural history of relapsed GBM following radiotherapy.

Discussion

Previous studies have demonstrated the feasibility and safety of administering PD-1 inhibition after CAR T-cell therapy in adult patients with lymphoma[23] and in adult patients with malignant pleural disease[24]. Concomitant administration of CAR T cells plus a PD-1 inhibitor has also been found to be safe in pediatric neuroblastoma[25]. We report the concomitant administration of CAR T-cell therapy and PD-1 inhibition for in adult patients with glioblastoma. The combination of EGFRvIII-targeted CAR T cells and pembrolizumab appeared safe and tolerable in this small cohort. However, despite confirmed reduction of target antigen following CAR T-cell administration in six out of seven

https://doi.org/10.1038/s43018-023-00709-6

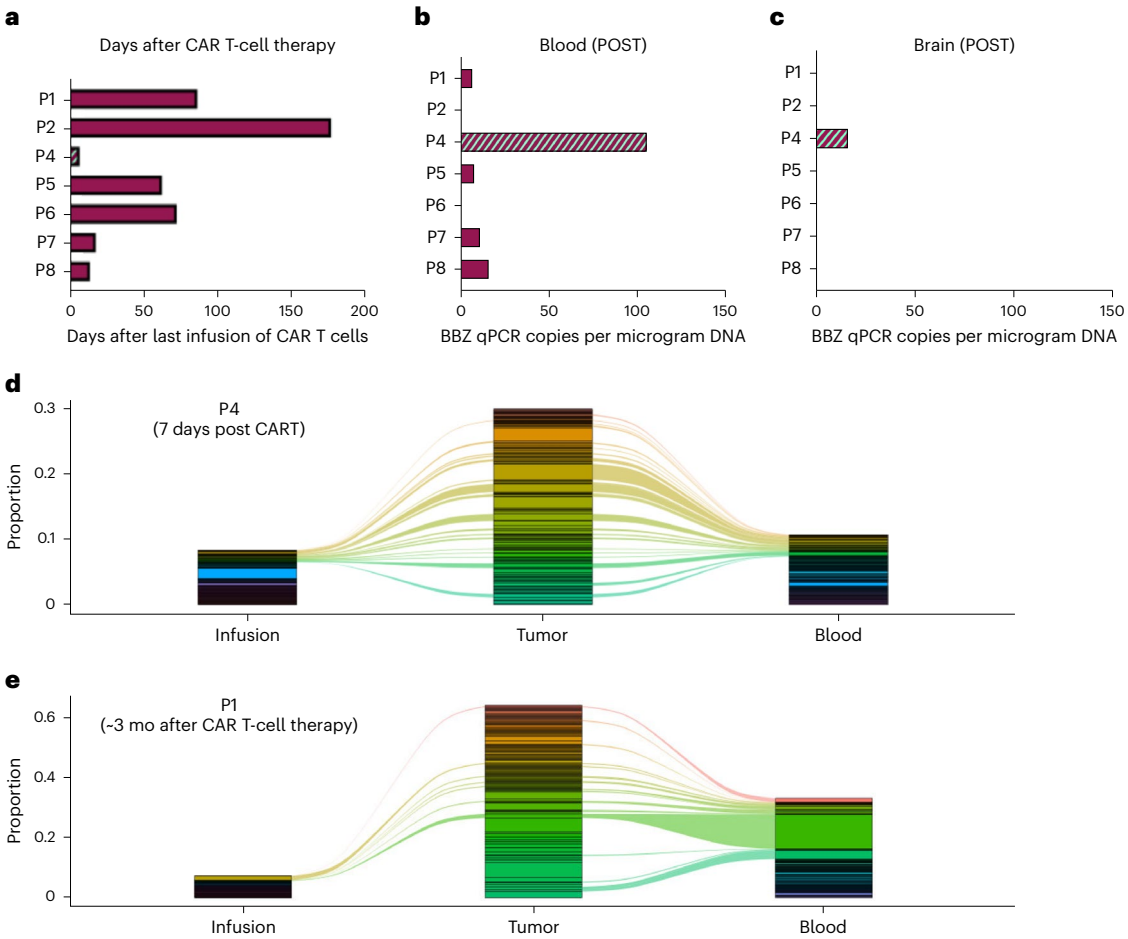

Fig. 3 | CAR T cells were detectable in one brain tumor after infusion. **a**, Barplot showing delay since last infusion of CAR T cells for each patient ($n = 7$). **b**, Barplot showing BBZ qPCR copies per microgram DNA for each patient in peripheral blood at the time of the relapse ($n = 7$). **c**, Barplot showing BBZ qPCR copies per microgram DNA for each patient in tumor samples harvested at the time of the relapse ($n = 7$). **d**, Comparison of the clonotypes found in the infusion product, the tumor (relapse, POST) and the peripheral blood (at the time of the relapse) for P4 (7 days after the first infusion of CAR T cells). **e**, Comparison of the clonotypes found in the infusion product, the tumor (relapse, POST), and the peripheral blood (at the time of the relapse) for P1 (~3 months after the last infusion of CAR T cells).

patients, a signal of clinical efficacy was not observed. Correspondingly, expansion and persistence of the CAR T cells in the blood was minimal, and repeated peripheral infusions of the CAR T-cell product did not augment peripheral engraftment. Although each infusion produced a spike in CAR T-cell copies detected in the blood, no meaningful expansion of infused cells was observed for any patient.

In an effort to better understand reasons for limited CAR T-cell expansion and clinical efficacy, we conducted correlative analyses on patient infusion products, peripheral blood samples and pre- and post-CAR T-cell tumor tissue samples. To be fully active, CAR T cells have to reach the tumor, and this step has been a challenge in solid tumors. Here, we confirmed in one patient our previous observation that EGFRvIII CAR T cells injected intravenously can potentially cross the blood-brain barrier and access the tumor[9]. However, whether the CAR T cells also penetrated the tumors in the other patients of the cohort remains unclear. The fact that we see substantial sharing of some TCRs among the infusion products and the tumor may indicate that the infusion product reached the tumor. However, we cannot rule out that these T cells infiltrated from the peripheral blood due to either pembrolizumab alone or the natural history of recurrent GBM. Regardless of their origin, bystander T cells from the infusion product and/or from the peripheral blood seem to have a longer persistence in the tumor as compared to the CAR T cells. Our hypothesis is that CAR T cells trafficked into the tumors but did not expand and persist, which may have contributed to the lack of clinical efficacy. Additional studies are needed to confirm this hypothesis.

There are many potential explanations for poor CAR T-cell expansion and persistence and resultant limited clinical efficacy in this study. First, it is possible that the decision to forego lymphodepleting chemotherapy, including temozolomide, played a pivotal role in the lack of clinical response. Lymphodepleting chemotherapy dramatically reduces circulating immune cell numbers and has been consistently demonstrated to enable better expansion and engraftment of the transferred T cells[26]. Although fractionated radiotherapy to the brain administered as standard of care in patients with GBM is lymphodepleting[27], it is likely inadequate for establishing an immune environment conducive to product expansion and persistence of peripherally delivered CAR T cells.

Another potential explanation for limited CAR T-cell expansion and clinical efficacy in this study may be limited encountering of the target antigen, in this case EGFRvIII, by the CAR T cells. Expression of EGFRvIII in GBM is highly heterogeneous, both spatially and temporally[18,28]. Although we attempted to address the issue of temporal heterogeneity by treating patients in the newly diagnosed setting, it is possible that there was loss of EGFRvIII expression in the tumors even in the first weeks following completion of first-line radiotherapy.

https://doi.org/10.1038/s43018-023-00709-6

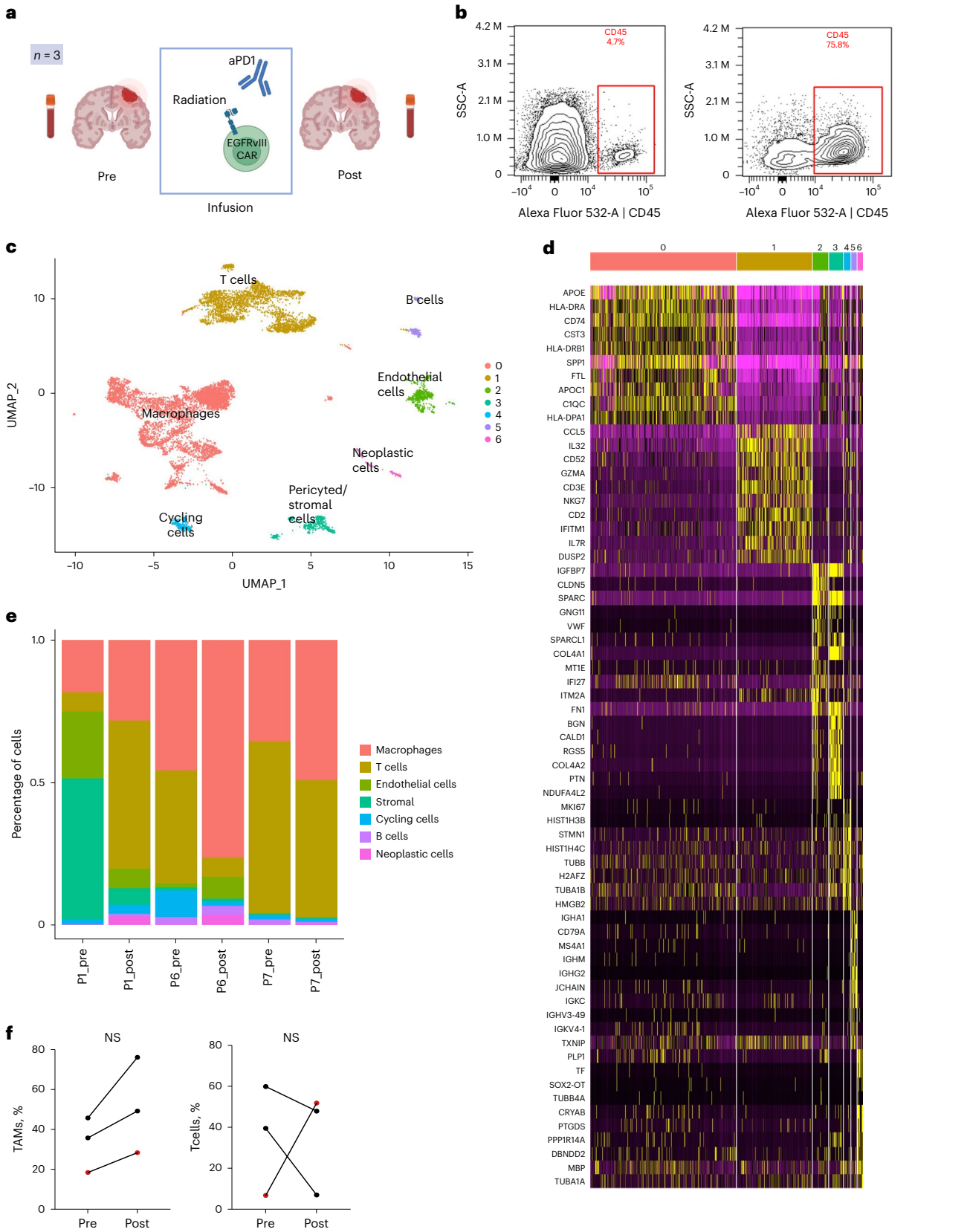

Fig. 4 | No major changes in the immune composition of the tumors overall. **a**, Tumor material was available for $n = 3$ patients before and after treatment. **b**, CD45 staining before (left) and after (right) CD45-based hematopoietic cells enrichment on a tumor sample. **c**, CD45-enriched cells were loaded on a 10x Genomics platform for scRNAseq and TCRseq. UMAP shows the overall cell space for the TME of three paired patients (three before and after CAR T infusion, with a total of six samples; 11,424 cells). **d**, Top 10 genes for each cluster as in panel c. **e**, Relative abundance of each cluster in each sample. **f**, Proportion of tumor-associated macrophages (TAMs) and T cells before and after treatment in the three paired patients (ratio paired *t*-test, two sided). Benjamini–Hochberg procedure was used to adjust for multiple comparisons.

https://doi.org/10.1038/s43018-023-00709-6

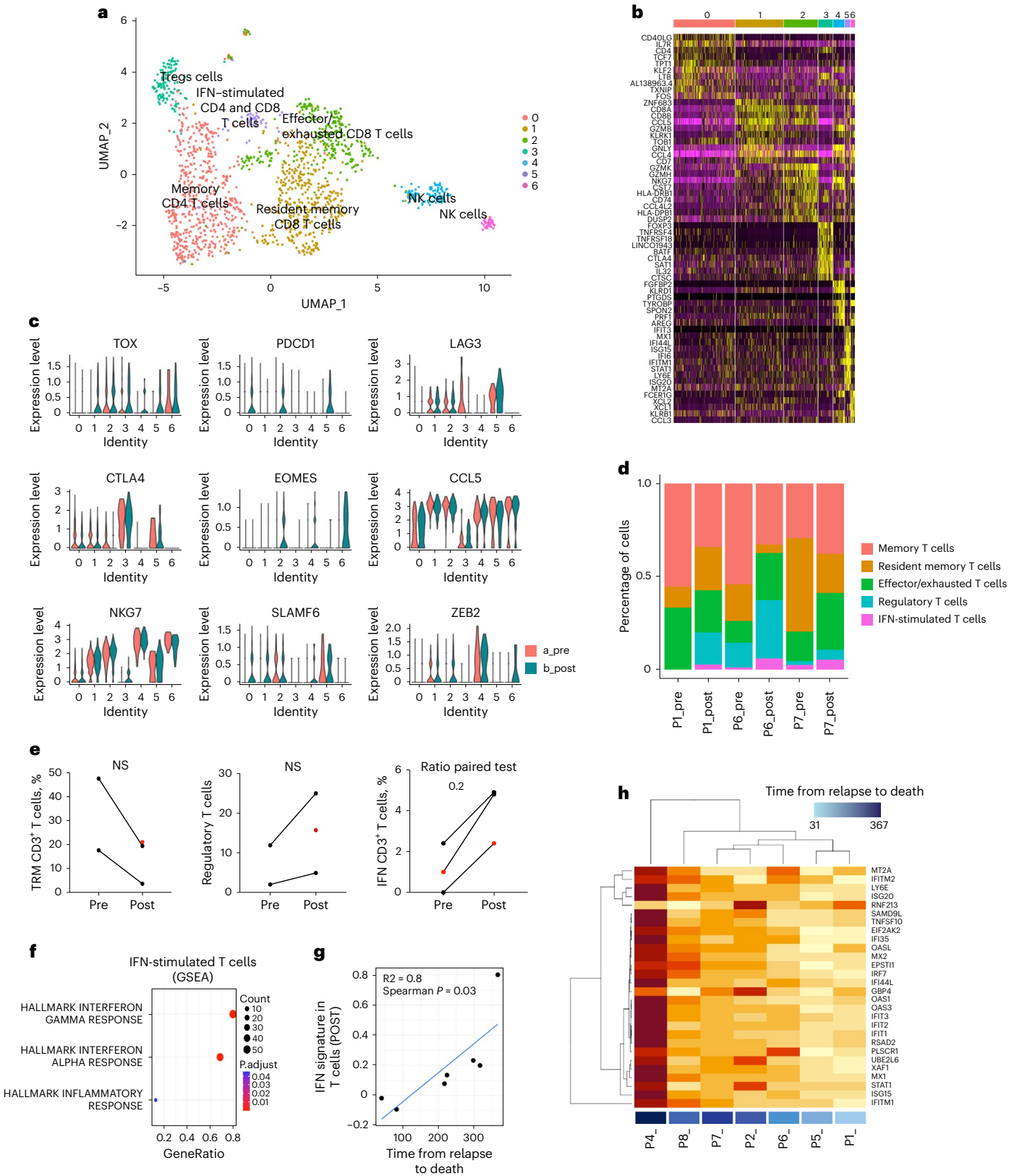

Fig. 5 | Increased T-cell exhaustion and IFN-stimulated T cells after treatment. **a**, UMAP shows the overall cell space for the TME of three paired patients (three before and three after therapy, for a total of six samples; 1,487 cells) after filtering T cells from the overall UMAP as in Fig. 4c. **b**, Top 10 genes for each cluster as in panel a. **c**, Violin plots show expression of genes before (Pre) and after (Post) CAR T-cell infusion in each cluster as in panel a. **d**, Relative abundance of each cluster in each sample. **e**, Proportion of TRM, TEX and IFN-stimulated T cells before and after treatment in the three paired patients (ratio paired *t*-test, two-sided). **f**, GSEA for the cluster of IFN-stimulated T cells. Benjamini–Hochberg procedure was used to adjust for multiple comparisons. **g**, Scatterplot shows the intensity of the IFN-signature in the seven patients at the time of the relapse as a function of time from relapse to death (Spearman correlation test, two sided). **h**, Heatmap shows the relative expression of the top genes in the IFN-stimulated T-cell cluster for each patient. Each patient is colored by the time from relapse to death.

Spatial heterogeneity was not directly addressed in this study but is the focus of newer generation products, including our ongoing trial of a bicistronic CAR (NCT05168423). In addition to heterogeneity, another target-related problem may have been that patients had too little gross residual tumor following surgery and radiation in the de novo treatment setting, resulting in inadequate target for the CAR T cells. Although there is evidence that CD19 CAR T cells can cross the blood-brain barrier and eliminate minimal central nervous system disease in patients with leukemia[29], the optimal amount of residual tumor for immunotherapy in GBM remains uncertain and likely varies depending on the exact immunotherapeutic modality[18,30]. It is also possible that the relatively low levels of EGFRvIII expression detected by NGS in most patients in this study contributed to the lack of CAR T-cell expansion and efficacy. This is also unclear, however, as prior studies have demonstrated that even ultra-low expression of target antigen may be adequate to trigger tumor cell elimination by CAR T cells[31].

Although we attempted to address PD-L1 upregulation with the addition of pembrolizumab, additional immunosuppressive mechanisms operative in the TME also likely hindered the CAR T-cell product. Our data suggest an increase in tumor-associated macrophages and regulatory T cells following treatment in the subset of patients in whom these cell populations were characterized before versus after CAR T-cell therapy. Additional therapeutic efforts will be needed to reduce the negative impact of these cell populations in future studies. It is also possible that additional immune checkpoints beyond PD-L1, as well as immunosuppressive cytokines and other soluble factors, were upregulated in the TME following infusion of CAR T-EGFRvIII cells and pembrolizumab. We aim to more broadly characterize the TME with additional analysis in subsequent studies. Of note, we previously reported a study of the GBM TME before and after standard-of-care treatment and demonstrated that the presence of IFN-stimulated T cells at the time of relapse was an important prognostic biomarker[22]. Here, we confirm this finding in a different cohort, under a different treatment regimen. This suggests that higher inflammation of the T-cell compartment is favorable to patients with GBM and should be pursued and/or monitored at the time of the relapse.

Lastly, it is also possible that concurrent administration of PD-1 blockade may have been deleterious to CAR T-cell expansion and/or function. Although we have previously demonstrated a correlation between PD-1 expression in the EGFRvIII CAR T-cell infusion product and peripheral engraftment and PFS in rGBM[17], this finding was not recapitulated in the current study, raising the possibility that PD-1 expression in the setting of CAR T-cell therapy for GBM is representative of activation and not terminal exhaustion. Prior preclinical studies have demonstrated mixed results for the combination of PD-1 inhibition with CAR T-cell therapy, with some showing clear benefit[32] and others demonstrating reduced CAR T-cell survival and diminished cytotoxity[33,34]. In the clinic, the addition of PD-1 blockade did not further enhance the accumulation or persistence of CAR T cells in patients with neuroblastoma (although no deleterious effects were noted)[25]. In patients with malignant pleural disease, the combination of pembrolizumab with regionally delivered mesothelin-targeted CAR T cells led to an efficacy signal with two patients achieving complete metabolic response on positron emission tomography scan[24]. Correlatives were unavailable to understand the specific impact of the PD-1 inhibitor. Overall, additional studies are needed to better elucidate the impact of PD-1 and PD-L1 inhibition, as well as inhibition of other immune checkpoints, in the context of CAR T-cell therapy for solid tumors.

In summary, EGFRvIII-targeted CAR T-cell therapy delivered intravenously in combination with pembrolizumab was safe and well tolerated in patients with de novo GBM. However, expansion and persistence of cells was minimal and no signal of clinical efficacy was observed. Potential explanations include a lack of lymphodepleting chemotherapy including no temozolomide administration, tumor heterogeneity and relatively low levels of EGFRvIII expression, too little residual tumor (that is, target) following surgery in the newly diagnosed setting, additional immunosuppressive elements of the TME and, potentially, the concomitant administration of a PD-1 inhibitor. Our experience suggests that alternative CAR T-cell products and/or combinatorial strategies are warranted to enhance CAR T-cell therapy for GBM.

Methods

Study design and treatment

The study was approved by the Institutional Review Board of the University of Pennsylvania and conducted according to the Declaration of Helsinki. The primary objective of this single-center, single-arm, open-label phase 1 study was to determine the safety and tolerability of repeated peripheral infusions of CAR T-EGFRVIII cells in combination with pembrolizumab. The study was designed to treat up to seven patients. The primary endpoint of safety, defined by the occurrence of treatment-related AEs, was assessed using the National Cancer Institute's Common Terminology Criteria for Adverse Events version v. 5.0. DLT was defined as grade ≥3 toxicity occurring within 21 days after cycle 1/day 1, which developed or worsened following dosing (not existent before study treatment), at least possibly related to CAR T-EGFRvIII cells and/or pembrolizumab and did not improve to grade ≤1 within 7 days of optimal medical management. Exceptions to this are outlined in the study protocol. Secondary endpoints included PFS and OS. PFS was defined as the number of days from the date of registration to confirmed disease progression per Modified Response Assessment in Neuro-Oncology criteria[35] or date of death from any cause, whichever occurred first, or censored at the date of last available tumor assessment. OS was defined as the number of days from the date of registration to death from any cause or censored at last known date alive. Exploratory/correlative endpoints included measurement of CAR T-EGFRvIII cells in peripheral blood and tumor tissue as well as assessment of the TME before versus after CAR T-cell therapy. A study schema is displayed in Fig. 1a. No sex-specific analyses were performed given the overall low sample size of the clinical trial. Further information on research design is available in the Nature Research Reporting Summary linked to this article.

Peripheral blood T cells collected by leukapheresis were stimulated and transduced with a lentiviral vector encoding the CAR: humanized anti-EGFRvIII single-chain variable fragment fused to the hinge and transmembrane domain of CD8 and the human 4-1BB and CD3ξ intracellular signaling domains[9]. CAR T-EGFRvIII cells were manufactured at the University of Pennsylvania Cell and Vaccine Production Facility under good manufacturing practices and then formulated and cryopreserved until the patient's first infusion. During manufacturing, patients received a hypofractionated course of radiation (40 Gy, 15 fractions) rather than standard full dose (60 Gy, 30 fractions) to minimize lymphocytotoxicity associated with external beam radiotherapy to the brain. Neither temozolomide nor lymphodepleting chemotherapy was administered. During a window of 2–3 weeks after the end of radiation, patients received a 200-mg pembrolizumab infusion followed 1 h later by CAR T cells (2×10^8 cells, 10–20 ml min^{-1}). In the absence of tumor progression or DLT and if $\geq 2 \times 10^7$ cells per dose were available, combination pembrolizumab + CAR T-EGFRvIII cell therapies were administered once every 3 weeks for up to three cycles, followed by a fourth and final cycle of pembrolizumab. Magnetic resonance imaging scans were performed 2–3 weeks following completion of radiotherapy and at least once every 6 weeks thereafter. For correlative studies, peripheral blood was collected on the day of leukapheresis, the first and last day of radiation, on days 1, 2, 4, 8, 11 and 15 of cycle 1, day 1 of each subsequent treatment cycle and at the end of study. Formalin-fixed paraffin-embedded tumor tissue samples were acquired for all patients from their initial GBM surgeries and from any subsequent resections performed after receiving CAR T-cell infusion.

A Data and Safety Monitoring Board (DSMB) comprising three individuals, including physicians with experience in oncology and/or

gene transfer therapy, was assembled and worked under a charter specifically developed for safety oversight of this study. The DSMB provided guidance to the sponsor and evaluated patient-subject safety as specified in the charter. The DSMB convened every 6 months throughout the study.

MGMT promoter methylation and EGFRvIII testing

MGMT promoter methylation status was determined in the Clinical Laboratory Improvement Amendments-certified Molecular Pathology Laboratory of the Hospital of the University of Pennsylvania. Bisulfite-converted DNA was amplified with primers targeting differentially methylated region 2 (DMR2) of the *MGMT* promoter, and percent methylation was determined by pyrosequencing of the amplified product (PyroMark Q24, Qiagen). To optimize turnaround time for trial enrollment, EGFRvIII positivity was determined by sending unstained slides with formalin-fixed paraffin-embedded tissue sections to NeoGenomics Laboratories for real-time quantitative RT-PCR. Expression of EGFRvIII was quantified by calculating the ratio of (EGFRvIII/EGFRvIII + wild-type EGFR) × 100.

CAR T-cell manufacturing

CAR T cells were manufactured as previously described[36]. Briefly, engineered CAR T cells were manufactured at the Cell and Vaccine Production Facility at the University of Pennsylvania, A Foundation for the Accreditation of Cellular Therapy-accredited facility. The leukapheresis product collected at the University of Pennsylvania Apheresis Center was processed at the Cell and Vaccine Production Facility to obtain the T-cell starting population. T cells were then activated and expanded using anti-CD3/28 conjugated paramagnetic microbeads (Life Technologies) followed by transduction with the lentiviral vector encoding the CAR construct. The construct was designed to include the 2173 single-chain variable fragment fused to the hinge and transmembrane domain of CD8 and the human 4-1BB and CD3ζ intracellular signaling domains. The lentiviral vector GMP manufacturing was completed at the City of Hope facility. The manufacturing cultures were maintained for approximately 9 days and harvested by washing and removal of the magnetic beads. The target dose was formulated and cryopreserved. The clinical doses were released for infusion upon passing all release testing for sterility, purity, identity and potency.

Blood processing

Whole blood from the patients was processed using a Ficoll gradient. Peripheral blood mononuclear cells were stored in DMSO 10% + FBS 20% media in liquid nitrogen until later use.

Brain tumor dissociation

Tumor biopsies before and after CAR T-EGFRvIII therapy were processed by mechanical and enzymatic dissociation using a gentleMACS Octo Dissociator in combination with the Brain Tumor Dissociation Kit (Miltenyi Biotec, 130-095-942) and then filtered through a 75-mm strainer to generate a single-cell suspension. Samples were frozen in liquid nitrogen until further use.

Measurement of transgene persistence in vivo by qRT-PCR

Quantification of transgene in the peripheral blood and tumor tissue was performed using qRT-PCR, as has been described previously[9]. Briefly, research sample processing, freezing and PCR were performed in the Translational and Correlative Studies Laboratory at the University of Pennsylvania, using established standard operating procedures. CAR T cells were quantified from peripheral blood samples obtained at protocol-specified time points. Peripheral blood samples were collected in lavender top (K2EDTA) Vacutainer tubes (Becton Dickinson) and delivered to the laboratory within 2 h of acquisition. Samples were processed within 16 h of acquisition, according to the established standard operating procedure. Genomic DNA was isolated directly from whole blood, and qRT-PCR analysis was performed using ABI TaqMan technology to detect the integrated CAR transgene sequence, using triplicates of 200 ng genomic DNA per timepoint for patient samples. To determine copy number per unit DNA, an eight-point standard curve was generated consisting of 5×10^6 copies of lentivirus plasmid spiked into 100 ng nontransduced control genomic DNA. The number of copies of plasmid present in the standard curve was verified using digital qPCR with the same primer/probe set and performed on a QuantStudio 3D digital PCR instrument (Life Technologies). For quality control checks, each datapoint (sample and standard curve) was evaluated in triplicate with a positive C_t value in three of three replicates. Additionally, the acceptable percent coefficient of variation was less than 0.95% for all quantifiable values. To control for the quality of interrogated DNA, we performed a parallel amplification reaction using 20 ng genomic DNA and a primer/probe combination specific for a nontranscribed genomic sequence upstream of the CDKN1A (p21) gene. These amplification reactions generated a correction factor to adjust for calculated versus actual DNA input. Copies of transgene per microgram of DNA were calculated according to the formula: copies per microgram of genomic DNA = (copies calculated from CAR T standard curve) × correction factor/(amount DNA evaluated in nanograms) × 1,000 ng.

CAR EGFRvIII detection by cytometry and at the RNA level

Identification of CAR^+ T cells in the peripheral blood and the infusion product was performed on single-cell suspensions using spectral cytometry. Briefly, thawed cells were resuspended in PBS-FBS 2% and then incubated with biotinylated EGFRvIII protein for 20 min at 4 °C before further staining with surface and intracellular antibodies as described below.

For identification of CAR^+ T cells in the scRNAseq data, Fastq files were processed using Cellranger version 6.0.0, which includes EmptyDrops method to identify population of cells with low RNA content. Cellranger count was run using a custom hg38/GRCh38 human genome reference including CAR T-cell specific genomic sequence to allow to detect CAR^+ T cells. This custom hg38/GRCh38 human genome reference was built according to the 10x Genomics protocol using cellranger mkref with the 10x Genomics-provided hg38/GRCh38 human reference genome (refdata-gex-GRCh38-2020-A).

Flow cytometry

Analytical flow cytometry was performed on patient infusion material as previously described[18]. Antibody information is provided in Supplementary Table 2. Gating strategy used to quantify $CD4^+CAR^+PD\text{-}1^+$ cell populations in displayed Extended Data Fig. 4.

Spectral cytometry

Thawed single-cell suspensions of infusion products were assessed using CyTek. Briefly, antibody panels (T-cell panel) were designed to simultaneously measure the expression of molecules related to cell lineage, differentiation state and function (Supplementary Table 1). Cells (3×10^6) were stained at 4 °C for 20 min with fluorochrome-labeled antibodies to detect surface proteins. Cells were then permeabilized using Fixation/Permeabilization solution (Thermo Fisher, 00-5523-00) at room temperature for 15 min and then stained at 4 °C for 30 min with fluorochrome-labeled antibodies to detect intracellular proteins. Cells were washed in permeabilization buffer and resuspended in PBS, FBS 2% paraformaldehyde before acquisition by CyTek. $CD45^+$ cells were identified as LiveDeadnegSingle$CD45^+$. Data were analyzed using OMIQ (https://www.omiq.ai/).

scRNAseq and TCRseq

Before running single-cell sequencing on brain samples, brain dissociation tissues were enriched using the EasySep Release Human CD45 Positive Selection Kit (StemCell, 100-0105). $CD45^+$ cells fraction were

resuspended in 1x PBS with 0.04% bovine serum albumin. Cell numbers and viability were measured using a Luna FL dual fluorescence cell counter as well as classical hemocytometer and trypan blue.

Before running single-cell on blood samples, peripheral blood mononuclear cells were enriched using the EasySep Human T Cell Enrichment Kit (StemCell, 19051). $CD3^+$ cells fraction were resuspended in 1x PBS with 0.04% bovine serum albumin. Cell numbers and viability were measured using a Luna FL dual fluorescence cell counter as well as classical hemocytometer and trypan blue.

Single-cell suspensions were loaded onto a Chromium Single Cell Chip (10x Genomics) according to the manufacturer's instructions for co-encapsulation with barcoded gel beads at a target capture rate of 10,000 individual cells per sample, based on the initial number of cells per sample. For all patients, RNA and TCR libraries were synthetized by following the Chromium Single Cell 5′ V(D)J Enrichment Kit, Human T Cell (10x Genomics).

Bioinformatic analysis

Data were collected using Cell Ranger software (10x Genomics) v2.0.1/v3.0.2 and analyzed using R v.3.5.1, and the following packages and versions in R for analysis: Seurat v3.1.1, ENHANCE v1.0.0, DropletUtils v1.8, clustree v0.4.1, and cluster v2.1.0. Two-dimensional gene expression maps were generated using coordinates from the UMAP algorithm using the R package uwot v0.1.3 implementation. Figures were produced using the following packages and versions in R: RColorBrewer v1.1-2, pheatmap v1.0.12, ggplot v3.2.0 and ggsignif v0.6.0.

Data analysis (scRNAseq and TCR)

Seurat v4.1.3 (ref. 37,38) was used for all subsequent analysis. We constructed a Seurat object using the filtered feature-barcode matrix for each sample after Cell Ranger analysis. A series of quality filters were applied to the data to remove cell barcodes: too few total transcript counts (<300); possible debris with too few genes expressed (<100); more than one cell with too many genes expressed (>5–10,000) and too many UMIs (>5–10,000); possible dead cell or a sign of cellular stress and apoptosis with too high proportion of mitochondrial gene expression over the total transcript counts (>10–20%). Each sample was scaled and normalized using Seurat's 'SCTransform' function (default parameters). We then merged all samples and repeated the same scaling and normalization method. All cells in the merged Seurat object were then integrated using Harmony[39,40] and then clustered via Seurat's 'FindNeighbors' and 'FindClusters' functions. The resulting merged and normalized matrix was used for subsequent analysis.

Cell types were assigned to each cluster by manually reviewing the expression of marker genes. Myeloid cluster was selected from overall UMAP/clustering, and cells expressing CD3D > 0 | CD3E > 0 | CD247 > 0 | JCHAIN > 0 | 'IGLV1-40' > 0 were filtered out. Lymphocytes/T cells were selected from overall UMAP/clustering and cells expressing CD68 ≤ 0 | CD163 ≤ 0 | CD14 ≤ 0, CD3D > 0 | CD3E > 0 | CD247 > 0, the proportion of transcripts that are of mitochondrial origin for every cell (percent.mt) < 10 or apoptotic cells were filtered out. Differentially expressed genes within tumor-associated macrophages, T cells and other cell types were identified by FindMarkers function comparing cells belonging to one subtype to the rest. Wilcoxon statistical test was used. Log_2 fold change > 0.25 and false discovery rate < 0.05 was used to filter differentially expressed genes. TCRseq data for each sample were processed using Cell Ranger software (versions as above), with the command 'cellranger vdj' using the human reference genome GRCh38. TCR analyses were performed using the scRepertoire package.

Statistics and reproducibility

Clinical trial data was stored in the Velos Clinical Trials Management System (Penn CTMS, v. 11.2.1.6) (WIRB-Copernicus Group). This was a single-center, single-arm, nonrandomized open-label phase 1 study. The statistical analysis for clinical data was primarily descriptive in keeping with the small sample size and exploratory nature of the study, which was limited to a sample size of seven patients due to budgetary constraints. No statistical method was used to predetermine sample size. Because no patients experienced DLT, the upper limit for the CI on DLT rate was calculated using the rule of three, whereby the interval from 0 to 3/n (number of subjects) is an approximate 95% CI for the DLT rate[41,42]. PFS was defined as the number of days from the date of registration to confirmed disease progression per Modified Response Assessment in Neuro-Oncology criteria or date of death from any cause, whichever occurred first, or censored at the date of last available tumor assessment. OS was defined as the number of days from the date of registration to death from any cause or censored at last known date alive. The survival function of PFS and OS were estimated by the Kaplan–Meier method[43]. Median PFS and OS time were calculated along with the associated 90% CIs. In evaluating EGFRvIII expression and EGFR amplification, the Wilcoxon matched-pairs signed-rank test was used to compare pre- versus post-CAR T-cell samples from the same patient. An unpaired *t*-test was used to compare PD-1 expression in the $CD4^+$/CAR^+ infusion product in patients with rGBM versus de novo GBM, and Spearman correlation was used to assess the relationship between PD-1 expression in the $CD4^+$/CAR^+ infusion product and CAR T-cell engraftment. $P < 0.05$ was considered significant. All statistical tests described were two-sided and performed using R version 4.1.2 (R Foundation for Statistical Computing). The swimmer's plot was generated using the *swimplot* package. No data were excluded from the analyses, and the experiments were not randomized. The investigators were not blinded to allocation during experiments and outcome assessment. Data distribution was assumed to be normal, but this was not formally tested.

Reporting summary

Further information on research design is available in the Nature Portfolio Reporting Summary linked to this article.

Data availability

scRNAseq and TCRseq data that support the findings of this study have been deposited in the Gene Expression Omnibus under accession code GSE242790. Source data for Figs. 1–5 and Extended Data Fig. 1 have been provided as source data files. All other data supporting the findings of this study including de-identified individual participant clinical data are available from the corresponding author upon reasonable request. Source data are provided with this paper.

Code availability

The scRNAseq and TCRseq analyses presented in the paper were performed with open-source algorithms as described in Methods. Further details will be made available by the authors on request. No custom code was generated in the course of this study.

References

1. van de Donk, N., Usmani, S. Z. & Yong, K. CAR T-cell therapy for multiple myeloma: state of the art and prospects. *Lancet Haematol.* **8**, e446–e461 (2021).
2. June, C. H. & Sadelain, M. Chimeric antigen receptor therapy. *N. Engl. J. Med.* **379**, 64–73 (2018).
3. Bagley, S. J. & O'Rourke, D. M. Clinical investigation of CAR T cells for solid tumors: Lessons learned and future directions. *Pharmacol. Ther.* **205**, 107419 (2020).
4. Hou, A. J. et al. Navigating CAR-T cells through the solid-tumour microenvironment.*Nat. Rev. Drug Discov.* **20**, 531–550 (2021).
5. Bagley, S. J. et al. CAR T-cell therapy for glioblastoma: recent clinical advances and future challenges. *Neuro. Oncol.* **20**, 1429–1438 (2018).
6. Ostrom, Q. T. et al. CBTRUS statistical report: primary brain and other central nervous system tumors diagnosed in the United States in 2013-2017. *Neuro. Onco.l* **22**, iv1–iv96 (2020).

7. Stupp, R. et al. Radiotherapy plus concomitant and adjuvant temozolomide for glioblastoma. *N. Engl. J. Med.* **352**, 987–996 (2005).
8. Wen, P. Y. et al. Glioblastoma in adults: a Society for Neuro-Oncology (SNO) and European Society of Neuro-Oncology (EANO) consensus review on current management and future directions. *Neuro. Oncol.* **22**, 1073–1113 (2020).
9. O'Rourke, D. M. et al. A single dose of peripherally infused EGFRvIII-directed CAR T cells mediates antigen loss and induces adaptive resistance in patients with recurrent glioblastoma. *Sci. Transl. Med.* **9**, eaaa0984 (2017).
10. Ahmed, N. et al. HER2-specific chimeric antigen receptor-modified virus-specific T cells for progressive glioblastoma: a phase 1 dose-escalation trial. *JAMA Oncol.* **3**, 1094–1101 (2017).
11. Brown, C. E. et al. Bioactivity and safety of IL13Rα2-redirected chimeric antigen receptor $CD8^+$ T cells in patients with recurrent glioblastoma. *Clin. Cancer Res.* **21**, 4062–4072 (2015).
12. Brown, C. E. et al. Regression of glioblastoma after chimeric antigen receptor T-cell therapy. *N. Engl. J. Med.* **375**, 2561–2569 (2016).
13. Durgin, J. S. et al. Case Report: Prolonged survival following EGFRvIII CAR T cell treatment for recurrent glioblastoma. *Front. Oncol.* **11**, 669071 (2021).
14. Felsberg, J. et al. Epidermal growth factor receptor variant III (EGFRvIII) positivity in EGFR-amplified glioblastomas: prognostic role and comparison between primary and recurrent tumors. *Clin. Cancer Res.* **23**, 6846–6855 (2017).
15. Li, G. & Wong, A. J. EGF receptor variant III as a target antigen for tumor immunotherapy. *Expert Rev. Vaccines* **7**, 977–985 (2008).
16. Koga, T. et al. Mapping of genomic EGFRvIII deletions in glioblastoma: insight into rearrangement mechanisms and biomarker development. *Neuro. Oncol.* **20**, 1310–1320 (2018).
17. Tang, O. Y. et al. PD1 expression in EGFRvIII-directed CAR T cell infusion product for glioblastoma is associated with clinical response. *Front. Immunol.* **13**, 872756 (2022).
18. Weller, M. et al. Rindopepimut with temozolomide for patients with newly diagnosed, EGFRvIII-expressing glioblastoma (ACT IV): a randomised, double-blind, international phase 3 trial. *Lancet Oncol.* **18**, 1373–1385 (2017).
19. Louis, D. N. et al. The 2021 WHO Classification of Tumors of the Central Nervous System: a summary. *Neuro. Oncol.* **23**, 1231–1251 (2021).
20. Fraietta, J. A. et al. Determinants of response and resistance to CD19 chimeric antigen receptor (CAR) T cell therapy of chronic lymphocytic leukemia. *Nat. Med.* **24**, 563–571 (2018).
21. Giles, J. R. et al. Human epigenetic and transcriptional T cell differentiation atlas for identifying functional T cell-specific enhancers. *Immunity* **55**, 557–574 (2022).
22. Alanio, C. et al. Immunologic features in de novo and recurrent glioblastoma are associated with survival outcomes. *Cancer Immunol. Res.* **10**, 800–810 (2022).
23. Chong, E. A. et al. Pembrolizumab for B-cell lymphomas relapsing after or refractory to CD19-directed CAR T-cell therapy. *Blood* **139**, 1026–1038 (2022).
24. Adusumilli, P. S. et al. A phase I trial of regional mesothelin-targeted CAR T-cell therapy in patients with malignant pleural disease, in combination with the anti-PD-1 agent pembrolizumab. *Cancer Discov.* **11**, 2748–2763 (2021).
25. Heczey, A. et al. CAR T cells administered in combination with lymphodepletion and PD-1 inhibition to patients with neuroblastoma. *Mol. Ther.* **25**, 2214–2224 (2017).
26. Amini, L. et al. Preparing for CAR T cell therapy: patient selection, bridging therapies and lymphodepletion. *Nat. Rev. Clin. Oncol.* **19**, 342–355 (2022).
27. Huang, J. et al. Clinical and dosimetric predictors of acute severe lymphopenia during radiation therapy and concurrent temozolomide for high-grade glioma. *Int. J. Radiat. Oncol. Biol. Phys.* **92**, 1000–1007 (2015).
28. Eskilsson, E. et al. EGFR heterogeneity and implications for therapeutic intervention in glioblastoma. *Neuro Oncol* **20**, 743–752 (2018).
29. Leahy, A. B. et al. CD19-targeted chimeric antigen receptor T-cell therapy for CNS relapsed or refractory acute lymphocytic leukaemia: a post-hoc analysis of pooled data from five clinical trials. *Lancet Haematol.* **8**, e711–e722 (2021).
30. Liau, L. M. et al. Association of autologous tumor lysate-loaded dendritic cell vaccination with extension of survival among patients with newly diagnosed and recurrent glioblastoma: a phase 3 prospective externally controlled cohort trial. *JAMA Oncol.* **9**, 112–121 (2023).
31. Nerreter, T. et al. Super-resolution microscopy reveals ultra-low CD19 expression on myeloma cells that triggers elimination by CD19 CAR-T. *Nat. Commun.* **10**, 3137 (2019).
32. Grosser, R. et al. Combination immunotherapy with CAR T cells and checkpoint blockade for the treatment of solid tumors. *Cancer Cell* **36**, 471–482 (2019).
33. Kalinin, R. S. et al. Engineered removal of PD-1 from the surface of CD19 CAR-T cells results in increased activation and diminished survival. *Front. Mol. Biosci.* **8**, 745286 (2021).
34. Wei, J. et al. PD-1 silencing impairs the anti-tumor function of chimeric antigen receptor modified T cells by inhibiting proliferation activity. *J. Immunother. Cancer* **7**, 209 (2019).
35. Ellingson, B. M., Wen, P. Y. & Cloughesy, T. F. Modified criteria for radiographic response assessment in glioblastoma cinical trials. *Neurotherapeutics* **14**, 307–320 (2017).
36. Garfall, A. L. et al. Anti-BCMA/CD19 CAR T cells with early immunomodulatory maintenance for multiple myeloma responding to initial or later-line therapy.*Blood Cancer Discov.* **4**, 118–133 (2023).
37. Butler, A. et al. Integrating single-cell transcriptomic data across different conditions, technologies, and species. *Nat. Biotechnol.* **36**, 411–420 (2018).
38. Hafemeister, C. & Satija, R. Normalization and variance stabilization of single-cell RNA-seq data using regularized negative binomial regression. *Genome Biol.* **20**, 296 (2019).
39. Korsunsky, I. et al. Fast, sensitive and accurate integration of single-cell data with Harmony. *Nat. Methods* **16**, 1289–1296 (2019).
40. Tran, H. T. N. et al. A benchmark of batch-effect correction methods for single-cell RNA sequencing data. *Genome Biol.* **21**, 12 (2020).
41. Hanley, J. A. & Lippman-Hand, A. If nothing goes wrong, is everything all right? Interpreting zero numerators. *JAMA* **249**, 1743–1745 (1983).
42. Eypasch, E. et al. Probability of adverse events that have not yet occurred: a statistical reminder. *Brit. Med. J.* **311**, 619–620 (1995).
43. Kaplan, E. L. & Meier, P. Nonparametric estimation from incomplete observations. *J. Am. Stat. Assoc.* **53**, 457–481 (1958).

Acknowledgements

We thank the patients who participated in this study and their families for their dedication to furthering GBM treatment. We also thank the Neurosurgery Clinical Research Division, J. Fraietta and the Translational and Correlative Sciences Laboratory and A. Brennan and the Clinical Cell and Vaccine Production Facility at the University of Pennsylvania Perelman School of Medicine for all of their clinical trial contributions and support. This work was funded by Novartis, the Abramson Cancer Center Glioblastoma Translational Center of Excellence, The Templeton Family Initiative in Neuro-Oncology, the Maria and Gabriele Troiano Brain Cancer Immunotherapy

Fund, the Parker Institute for Cancer Immunotherapy (PICI Award Number C-01919), a public grant overseen by the French National Research Agency (Agence Nationale de la Recherche (ANR)) as part of the Investment Programme France 2030 under grant agreement ANR-21-RHUS-0016, and the French National Cancer Institute, the Ministry of Health and Prevention and Interm. High-throughput sequencing was performed by the ICGex NGS platform of the Institut Curie supported by the grants ANR-10-EQPX-03 (Equipex) and ANR-10-INBS-09-08 (France Génomique Consortium) from the ANR ("Investissements d'Avenir" program), by the ITMO-Cancer Aviesan (Plan Cancer III) and by the SiRIC-Curie program (SiRIC Grant INCa-DGOS-465 and INCa-DGOS- Inserm_12554). We also acknowledge ANR-10-IDEX-0001-02 PSL, CIC IGR-Curie 1428, INCa-DGOS-Inserm-ITMO cancer_18000 and LabEx DCBIOL. We thank the Parker Institute for Cancer Immunotherapy members for all of their constructive feedback, as well as Clinical Immunology laboratory and U932 at the Institut Curie (Paris, France) for insightful discussions, O. Lantz for critical feedback on the ancillary work, N. Amzallag for her support and the genomic and cytometry platforms of Institut Curie for their help.

Author contributions

S.J.B., A.S.D., E.M., A.M., J.L.B., E.H. and D.M.O. designed the study. S.J.B., A.S.D., E.M., S.B., R.L., G.K., M.A.B., S.M., E.H. and D.M.O. recruited and treated patients in the study. L.L., C.A., Z.A.B., M.P.N., S.K., W.T.H., O.Y.T., M.L., M.B., K.M. and D.D. generated, curated and analyzed data. C.A.,P.E.B., C.G., W.R., E.M., D.M., E.P. and J.J.W. performed bioinformatic analyses. S.J.B., Z.A.B.,L.L. and C.A. wrote the original paper, and S.J.B., Z.A.B., L.L., M.P.N., S.B., S.M., S.K., E.J.W, W.T.H., O.Y.T.,E.P,.J.J.W., S.A.,D.M., G.L.B., J.L.B., C.A. and D.M.O. reviewed and edited the paper. S.J.B., Z.A.B., G.L.B., E.J.W., D.M., C.A. and D.M.O. supervised the study. Funding support was provided by C.A. and J.L.B. C.A. and D.M.O. contributed equally to this study.

Competing interests

S.J.B. has received consulting fees from Kiyatec, Novocure and Bayer and has received research funding from Incyte, Tmunity, Novocure, GSK and Eli Lilly, all outside of the submitted work. S.J.B., A.S.D. and D.M.O. have inventorship interest in intellectual property owned by Novartis and the University of Pennsylvania: U.S. patent 62/809,245: "Combination therapies of EGFRvIII CARs and PD-1 inhibitors". Z.A.B. has inventorship interest in intellectual property owned by the University of Pennsylvania and has received royalties related to CAR T-cell therapy in solid tumors. S.M. has received consulting fees from AI Integrated Radiological Solutions Medial and Qynapse SAS and has received research funding from Novocure and Galileo CDS, all outside of the submitted work. G.L.B. has received consulting fees from Seattle Genetics (now Seagen), Adicet Bio, Aduro Biotech, AstraZeneca, BiolineRx, BioMarin Pharmaceuticals, Bristol-Myers Squibb, Cantargia, Cour Pharmaceuticals, Boehinger Ingelheim, Genmab, Hibercell, HotSpot Therapeutics, Incyte Corporation, Janssen, Merck, Molecular Partners, NanoGhost, Pancreatic Cancer Action Network, Shattuck Labs and Verastem and reports receiving research funding from Incyte Corporation, Bristol-Myers Squibb, Verastem, Halozyme, Biothera, Newlink, Novartis, Arcus Biosciences and Janssen, all outside of the submitted work. E.J.W. receives honoraria and/or research support from BMS, Merck, MedImmune, Surface Oncology, Takeda and KyMab. E.J.W. has a patent licensing agreement for the PD-1 pathway. J.L.B. reports employment with, is a current holder of stock options and holds patents with Novartis Institutes for Biomedical Research. D.M. is inventor of patents in the field of cell and gene therapy filed by the University of Pennsylvania and the University of Geneva, is scientific co-founder of Cellula Therapeutics and is a member of the scientific advisory board of MPC, Limula and Cellula Therapeutics. D.M.O. has received consulting fees from Celldex Therapeutics, Prescient Therapeutics and Century Therapeutics; has received research funding from Celldex Therapeutics, Novartis and Tmunity Therapeutics; and is an inventor of intellectual property (U.S. patent numbers 7,625,558 and 6,417,168 and related families) and has received royalties related to targeted ErbB therapy in solid cancers previously licensed by the University of Pennsylvania. C.A. is a consultant for Biotherapy Partners. All other authors declare no competing interests.

Additional information

Extended data is available for this paper at https://doi.org/10.1038/s43018-023-00709-6.

Supplementary information The online version contains supplementary material available at https://doi.org/10.1038/s43018-023-00709-6.

Correspondence and requests for materials should be addressed to Stephen J. Bagley or Cecile Alanio.

Peer review information *Nature Cancer* thanks Jon Amund Kyte, Wendy London, Julie Park and Mario Suva for their contribution to the peer review of this work.

Reprints and permissions information is available at www.nature.com/reprints.

Publisher's note Springer Nature remains neutral with regard to jurisdictional claims in published maps and institutional affiliations.

[1]Department of Medicine, Perelman School of Medicine at the University of Pennsylvania, Philadelphia, PA, USA. [2]Department of Neurosurgery, Perelman School of Medicine at the University of Pennsylvania, Philadelphia, PA, USA. [3]Center for Cellular Immunotherapies, Perelman School of Medicine at the University of Pennsylvania, Philadelphia, PA, USA. [4]GBM Translational Center of Excellence, Abramson Cancer Center, Perelman School of Medicine at the University of Pennsylvania, Philadelphia, PA, USA. [5]Clinical Immunology Laboratory, Institut Curie, Paris, France. [6]INSERM U932, PSL University, Immunity and Cancer, Institut Curie Research Center, Paris, France. [7]Parker Institute for Cancer Immunotherapy, San Francisco, CA, USA. [8]Agora Cancer Research Center, Lausanne, Switzerland. [9]Center for Translational Research in Onco-Hematology, University of Geneva, Geneva, Switzerland. [10]Swiss Cancer Center Léman, Lausanne and Geneva, Geneva, Switzerland. [11]Department of Oncology, University Hospital of Geneva, Geneva, Switzerland. [12]Department of Pathology and Laboratory Medicine, Perelman School of Medicine at the University of Pennsylvania, Philadelphia, PA, USA. [13]Department of Radiation Oncology, Perelman School of Medicine at the University of Pennsylvania, Philadelphia, PA, USA. [14]Department of Translational Research, PSL Research University, Institut Curie Research Center, Paris, France. [15]Department of Hematology and Medical Oncology, Emory University, Atlanta, GA, USA. [16]Cytometry Platform, CurieCoreTech, Institut Curie, Paris, France. [17]INSERM U830, PSL University, Institut Curie Research Cente, Paris, France. [18]Department of Radiology, Perelman School of Medicine at the University of Pennsylvania, Philadelphia, PA, USA. [19]Department of Biostatistics,

Epidemiology, and Informatics, Perelman School of Medicine at the University of Pennsylvania, Philadelphia, PA, USA. [20]Warren Alpert Medical School of Brown University, Providence, RI, USA. [21]Cooper Medical School of Rowan University, Camden, NJ, USA. [22]Department of Systems Pharmacology and Translational Therapeutics, Perelman School of Medicine, University of Pennsylvania, Philadelphia, PA, USA. [23]Institute for Immunology and Immune Health, Cambridge, MA, USA. [24]Novartis Institutes for BioMedical Research, Cambridge, MA, USA. [25]These authors contributed equally: S. J. Bagley, Z. A. Binder, L. Lamrani. ✉e-mail: sbagley@pennmedicine.upenn.edu; cecile.alanio@curie.fr

https://doi.org/10.1038/s43018-023-00709-6

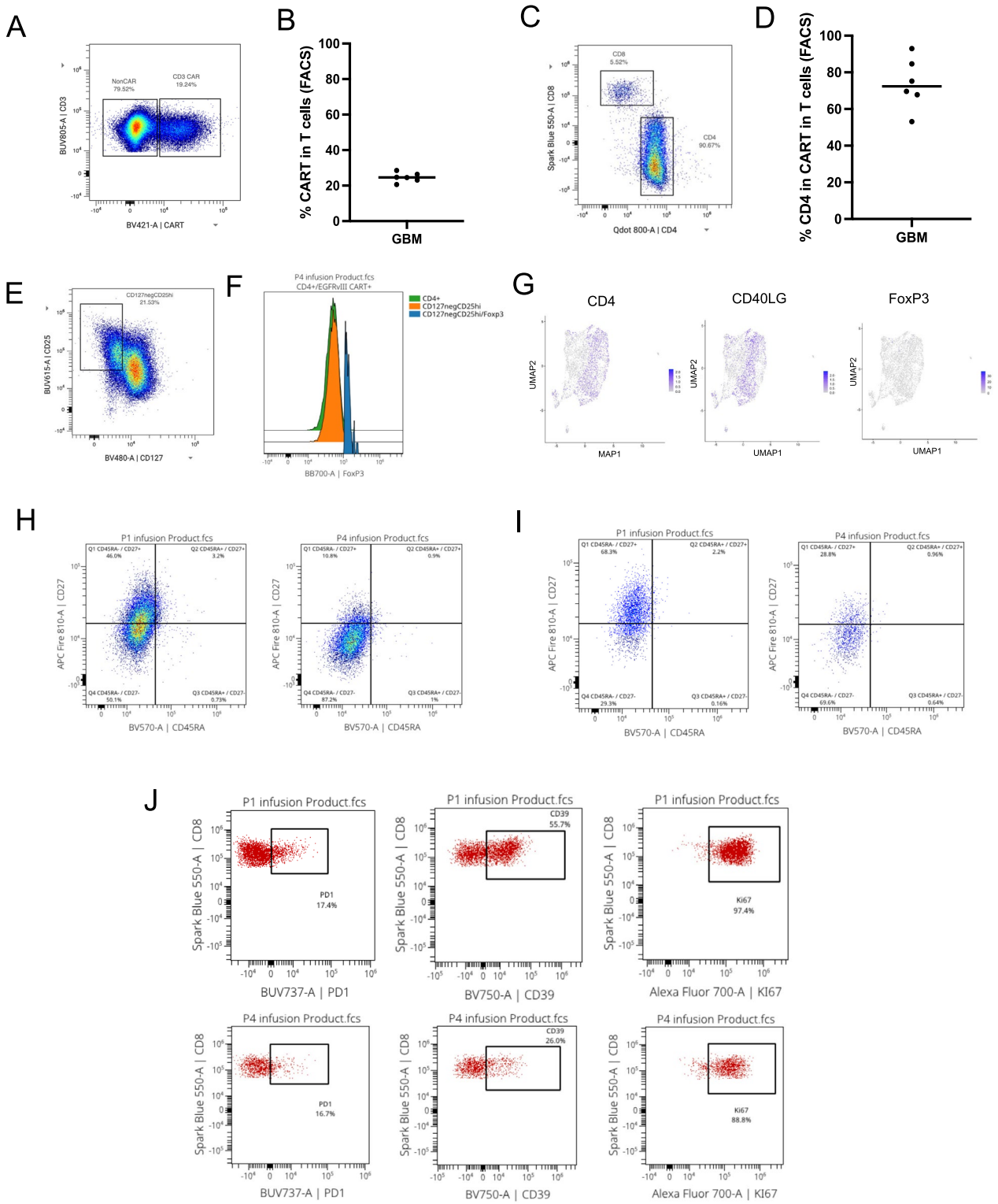

Extended Data Fig. 1 | See next page for caption.

https://doi.org/10.1038/s43018-023-00709-6

Extended Data Fig. 1 | CAR T cells in the infusion products are activated and exhausted effector T cells, with comparable features across patients. **(a)** Representative example of EGFRvIII CAR T cells staining in the infusion product. **(b)** Scatterplot shows proportion of EGFRvIII CAR T cells staining in the infusion products of the patients. **(c)** Representative example of CD4/CD8 staining in EGFRvIII CAR T cells staining in the infusion product. **(d)** Scatterplot shows proportion of CD4 T cells within EGFRvIII CAR T cells in the infusion products of the patients. **(e)** Representative example of CD127/CD25 regulatory T cells staining in the infusion product. **(f)** Representative example of Foxp3 expression in the different CD4 T-cell subsets in the infusion product. **(g)** Expression of CD4, CD40LG, Foxp3 in the infusion product as detected by RNA in scRNAseq data projected on a UMAP. **(h)** Representative example of CD45RA/CD127 staining in CD4 CAR T cells in the infusion product (P1, left; P4, right). **(i)** Representative example of CD45RA/CD127 staining in CD8 CAR T cells in the infusion product (P1, left; P4, right). **(j)** Representative example of PD1, CD39, Ki67 staining in CD8 T cells in the infusion product (P1, top; P4, bottom). **(k)** Heatmap shows expression in CD8 T cells in the infusion product of P1 and P4 as compared to a normal donor.

https://doi.org/10.1038/s43018-023-00709-6

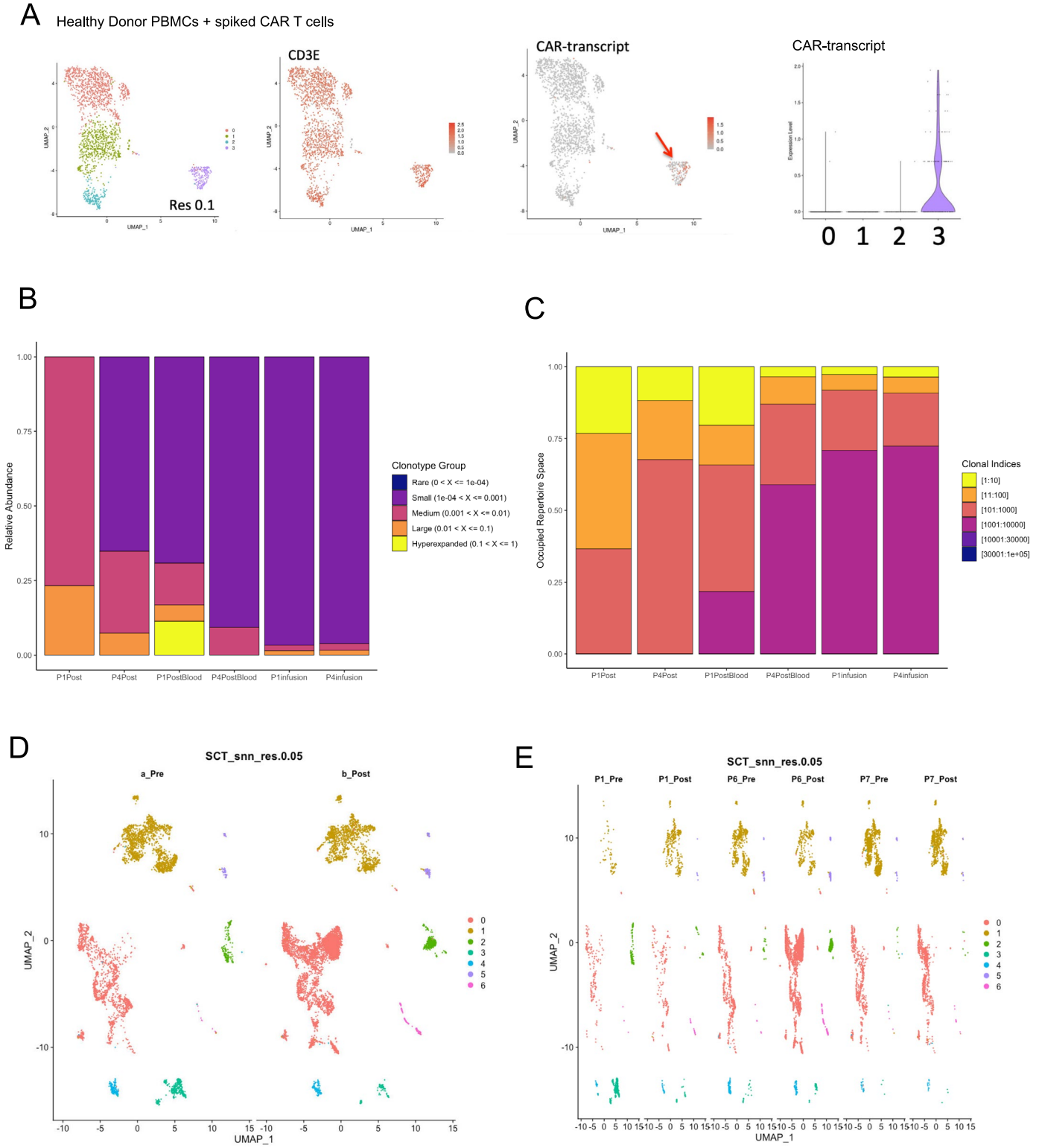

Extended Data Fig. 2 | Bioinformatic analysis. (a) Example of our strategy for detecting CAR T cells by RNA on scRNAseq data, here applied to one healthy donor where we spiked small amount of CAR T cells. **(b)** Clonal space homeostasis indicating percentage of clones in distinct proportions in the six paired samples. **(c)** Clonal Proportion where clonotypes are ranked by copy or frequency of occurrence in the six paired samples. **(d)** UMAP shows the overall cell space for the TME of three paired patients as in Fig. 4c, here split by 3 Pre (left) and 3 Post (right). **(e)** UMAP shows the overall cell space for the TME of three paired patients as in Fig. 4c, here split by sample.

https://doi.org/10.1038/s43018-023-00709-6

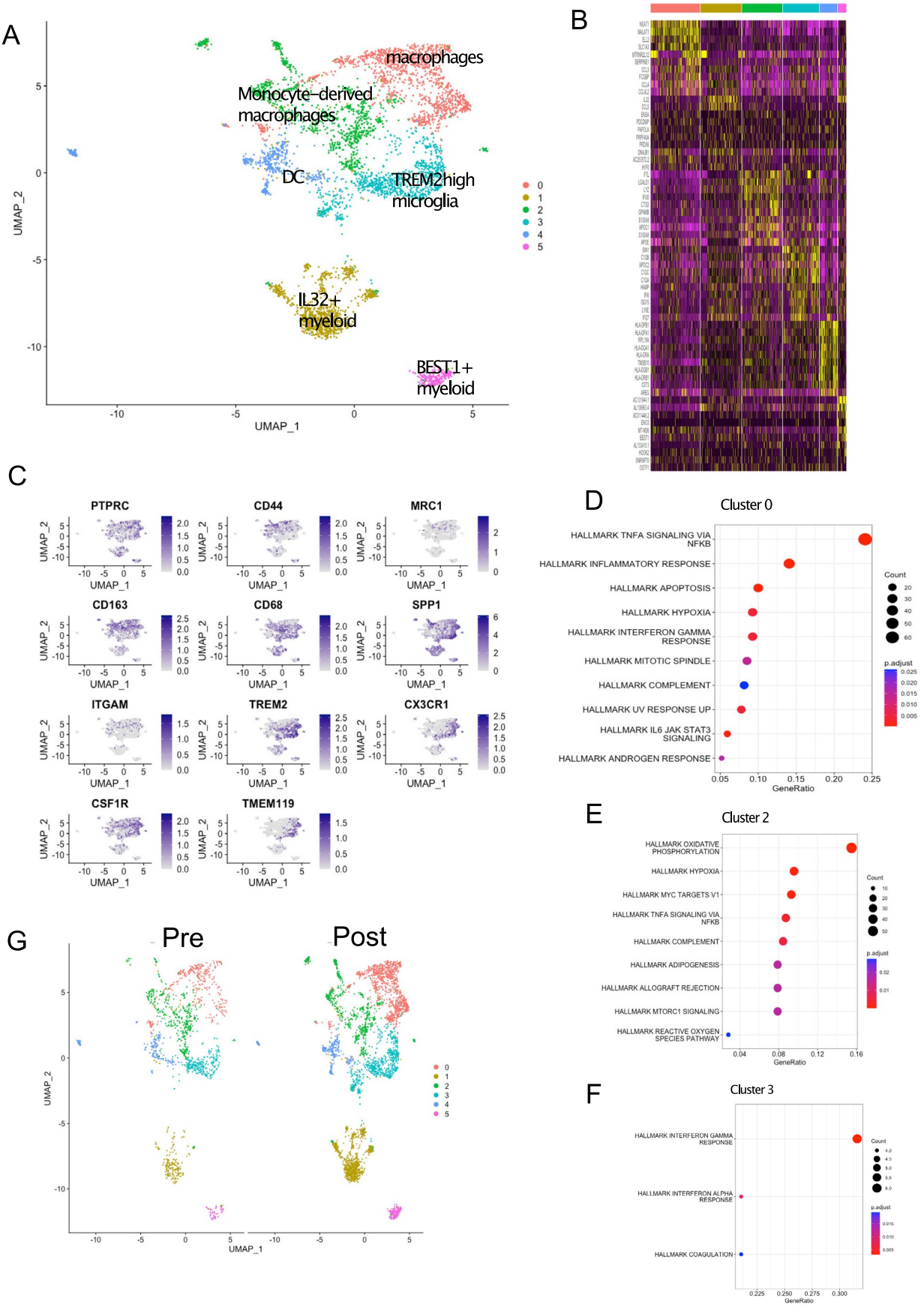

Extended Data Fig. 3 | See next page for caption.

https://doi.org/10.1038/s43018-023-00709-6

Extended Data Fig. 3 | Increased myeloid inflammation with therapy. **(a)** UMAP shows the overall cell space for the TME of three paired patients (3 Pre and Post, total six samples) after filtering myeloid cells from the overall UMAP as in Fig. 4c. **(b)** Top 10 genes for each cluster as in A. **(c)** Gene expression on top of each cluster as in A. GSEA of cluster 0 (**d**), 2 (**e**), and 3 (**f**) as defined in A. GSEA employs a permutation-based test usng Kolmogorov-Smirnov; Benjamini-Hochberg procedure was used to adjust for multiple comparisons. **(g)** UMAP shows the overall cell space for the myeloid TME of three paired patients as in A, here split by 3 Pre (left) and 3 Post (right).

https://doi.org/10.1038/s43018-023-00709-6

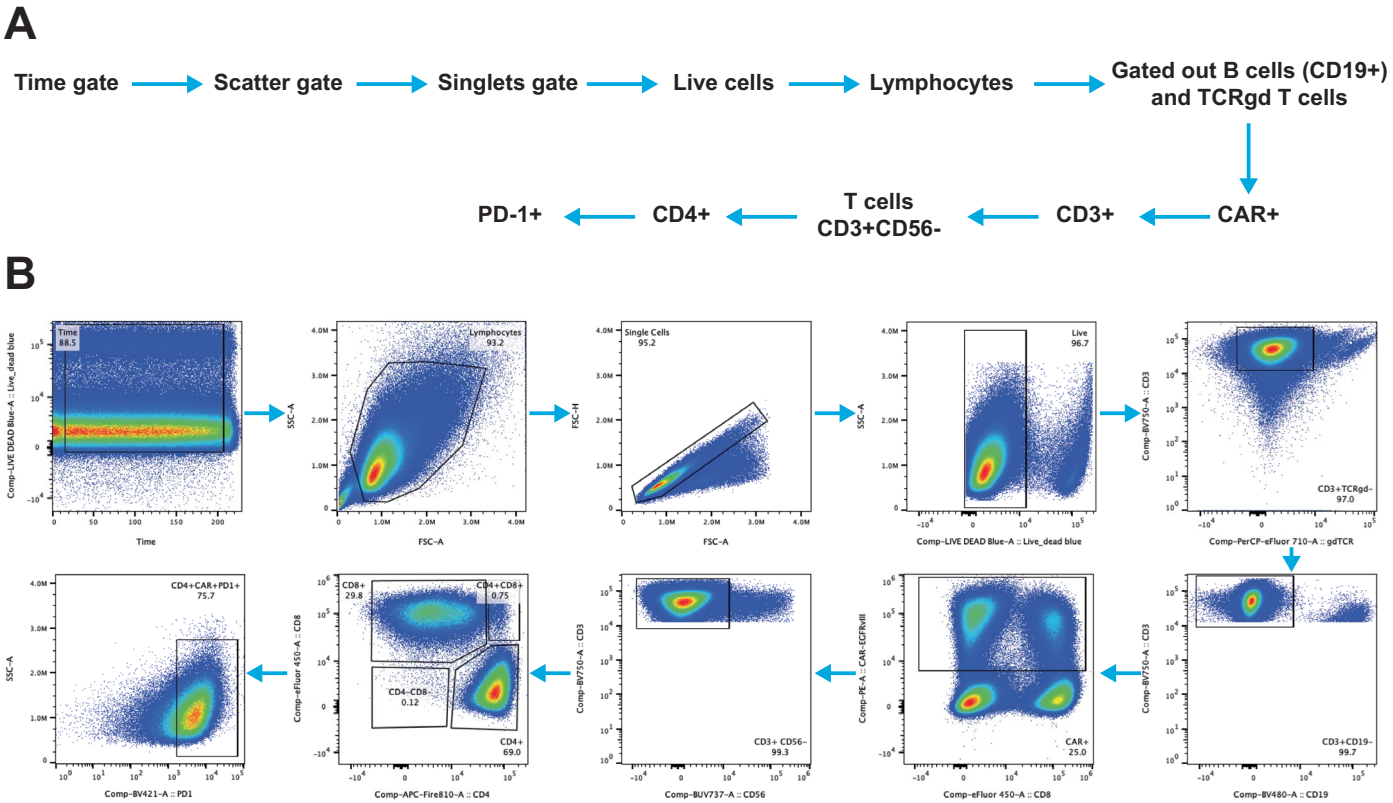

Extended Data Fig. 4 | Flow cytometry analysis of PD-1 expression. (a) Flow cytometry gating schema for quantification of $CD4^+/CAR^+$ PD-1 expression in infusion product. **(b)** Exemplary flow cytometry plots taken from 6 total samples.

nature portfolio

Corresponding author(s): Stephen J. Bagley, MD, MSCE

Last updated by author(s): Dec 12, 2023

Reporting Summary

Nature Portfolio wishes to improve the reproducibility of the work that we publish. This form provides structure for consistency and transparency in reporting. For further information on Nature Portfolio policies, see our Editorial Policies and the Editorial Policy Checklist.

Statistics

For all statistical analyses, confirm that the following items are present in the figure legend, table legend, main text, or Methods section.

n/a	Confirmed
☐	☒ The exact sample size (*n*) for each experimental group/condition, given as a discrete number and unit of measurement
☒	☐ A statement on whether measurements were taken from distinct samples or whether the same sample was measured repeatedly
☐	☒ The statistical test(s) used AND whether they are one- or two-sided *Only common tests should be described solely by name; describe more complex techniques in the Methods section.*
☒	☐ A description of all covariates tested
☒	☐ A description of any assumptions or corrections, such as tests of normality and adjustment for multiple comparisons
☐	☒ A full description of the statistical parameters including central tendency (e.g. means) or other basic estimates (e.g. regression coefficient) AND variation (e.g. standard deviation) or associated estimates of uncertainty (e.g. confidence intervals)
☐	☒ For null hypothesis testing, the test statistic (e.g. *F*, *t*, *r*) with confidence intervals, effect sizes, degrees of freedom and *P* value noted *Give P values as exact values whenever suitable.*
☒	☐ For Bayesian analysis, information on the choice of priors and Markov chain Monte Carlo settings
☒	☐ For hierarchical and complex designs, identification of the appropriate level for tests and full reporting of outcomes
☒	☐ Estimates of effect sizes (e.g. Cohen's *d*, Pearson's *r*), indicating how they were calculated

Our web collection on statistics for biologists contains articles on many of the points above.

Software and code

Policy information about availability of computer code

Data collection	Velos (WIRB-Copernicus Group; PennCTMS v11.2.1.6); Cell Ranger software (10X Genomics) v2.0.1/v3.0.2
Data analysis	R versions 3.5.1 and 4.1.2 (R Foundation for Statistical Computing, Vienna, Austria); OMIQ (https://www.omiq.ai/); Seurat v3.1.1, ENHANCE v1.0.0, DropletUtils v1.8, clustree v0.4.1, and cluster v2.1.0 two-dimensional gene expression maps, were generated using coordinates from the Uniform Manifold Approximation and Projection (UMAP) algorithm using the R package uwot v0.1.3 implementation; Figures were produced using the following packages and versions in R: RColorBrewer v1.1-2, pheatmap v1.0.12, ggplot v3.2.0, and ggsignif v0.6.0; Seurat v4.1.3 was used for all scRNAseq analyses. TCR-seq data for each sample were processed using Cell Ranger software (versions as above), with the command "cellranger vdj" using the human reference genome GRCh38. TCR analyses were performed using the scRepertoire package.

For manuscripts utilizing custom algorithms or software that are central to the research but not yet described in published literature, software must be made available to editors and reviewers. We strongly encourage code deposition in a community repository (e.g. GitHub). See the Nature Portfolio guidelines for submitting code & software for further information.

Data

Policy information about availability of data

All manuscripts must include a data availability statement. This statement should provide the following information, where applicable:

- Accession codes, unique identifiers, or web links for publicly available datasets
- A description of any restrictions on data availability
- For clinical datasets or third party data, please ensure that the statement adheres to our policy

The data that support the findings of this study are included in the paper or available from the corresponding author upon reasonable request. Further information on research design is available in the Nature Research Reporting Summary linked to this article. Source data for Figs. 1–5 and Supplementary Fig. 1 have been provided as Source Data files. Source data are provided with this paper. The authors will share de-identified individual participant clinical data that underlie the results reported in this manuscript upon reasonable request.

Research involving human participants, their data, or biological material

Policy information about studies with human participants or human data. See also policy information about sex, gender (identity/presentation), and sexual orientation and race, ethnicity and racism.

Reporting on sex and gender	Sex was collected as a baseline characteristic of each participant. No sex-specific analyses were performed given the overall low sample size of the clinical trial.
Reporting on race, ethnicity, or other socially relevant groupings	Race and ethnicity were self-reported by the study participants. Categories participants could choose from included: Race: Caucasian, Black or African American, Asian, American Indian or Alaska Native, or Native Hawaiian or other Pacific Islander Ethnicity: Hispanic vs. Non-Hispanic
Population characteristics	Median age 63 (IQR, 59-76) Sex: 2 female, 5 male Race/ethnicity: all participants were white/non-hispanic Diagnosis and prior treatments: all 7 participants had diagnosis of glioblastoma, IDH-wild type and were newly diagnosed with no prior therapies.
Recruitment	Potential study candidates were recruited from the neuro-oncology clinical practice at the Hospital of the University of Pennsylvania. Patients with newly diagnosed, previously untreated glioblastoma that had been surgically biopsied or resected and who met the study's inclusion/exclusion criteria (as outlined in the study protocol) were approached to sign informed consent for the study. It is possible that patients who elected to enroll on this trial may have better overall health, performance status, and psychosocial support relative to the general population of patients diagnosed with glioblastoma. However, as described in the manuscript, this small, single-arm study did not demonstrate any signal of efficacy. Thus, selection bias is not relevant in interpreting the results of this trial.
Ethics oversight	This study was approved by University of Pennsylvania Institutional Review Board

Note that full information on the approval of the study protocol must also be provided in the manuscript.

Field-specific reporting

Please select the one below that is the best fit for your research. If you are not sure, read the appropriate sections before making your selection.

☒ Life sciences ☐ Behavioural & social sciences ☐ Ecological, evolutionary & environmental sciences

For a reference copy of the document with all sections, see nature.com/documents/nr-reporting-summary-flat.pdf

Life sciences study design

All studies must disclose on these points even when the disclosure is negative.

Sample size	The sample size for this phase 1 safety and feasibility study was based on feasibility and budgetary constraints.
Data exclusions	No data were excluded from the analyses.
Replication	All attempts at replication were successful.
Randomization	This was a single-arm study.
Blinding	This was a single-arm study.

Reporting for specific materials, systems and methods

We require information from authors about some types of materials, experimental systems and methods used in many studies. Here, indicate whether each material, system or method listed is relevant to your study. If you are not sure if a list item applies to your research, read the appropriate section before selecting a response.

Materials & experimental systems

n/a	Involved in the study
☐	☒ Antibodies
☒	☐ Eukaryotic cell lines
☒	☐ Palaeontology and archaeology
☒	☐ Animals and other organisms
☐	☒ Clinical data
☒	☐ Dual use research of concern
☒	☐ Plants

Methods

n/a	Involved in the study
☒	☐ ChIP-seq
☐	☒ Flow cytometry
☐	☒ MRI-based neuroimaging

Antibodies

Antibodies used

CD45 Spectral Human Mouse HI30 AF532 1:100 FisherScientific 15560387
CD69 Spectral Human Mouse FN50 eFluor 450 1:200 FisherScientific 15568573
TCF1 Spectral Human Rabbit C63D9 AF647 1:400 Cell Signaling 6709S
LAG3 Spectral Human Mouse 3DS223H AF660 1:100 FisherScientific 17166228
KI67 Spectral Human Mouse B56 AF700 1:50 BD Biosciences 561277
CD27 Spectral Human Mouse QA17A18 APC Fire 810 1:400 Biolegend 393213
4-1BB Spectral Human Mouse 4B4 (4B4-1) APC efluor 780 1:800 FisherScientific 17123913
CD38 Spectral Human Mouse HIT2 BB515 1:200 BD Biosciences 564499
Tigit Spectral Human Mouse MBSA43 PerCP Efluor710 1:50 FisherScientific 15549426
CD28 Spectral Human Mouse CD28.2 BUV395 1:50 BD Biosciences 740308
CXCR5 Spectral Human Rat LOU RF8B2 BUV563 1:800 BD Biosciences 741316
CD25 Spectral Human Mouse 2A3 BUV615 1:200 BD Biosciences 612996
CD226 Spectral Human Mouse DX11 BUV661 1:400 BD Biosciences 749934
PD-1 Spectral Human Mouse EH12.1 BUV737 1:100 BD Biosciences 612792
CD3 Spectral Human Mouse HIT3a BUV805 1:200 BD Biosciences 741999
EOMES Spectral Human Mouse WD1928 PE-eFluor610 1:50 FisherScientific 15500517
CD127 Spectral Human Mouse HIL-7R-M21 BV480 1:50 BD Biosciences 566158
CD19 Spectral Human Mouse SJ25C1 BV510 1:200 BD Biosciences 562947
LIVE/DEAD Blue Spectral N/A N/A N/A N/A 1:1000 BD Biosciences 564406
CD41a Spectral Human Mouse HIP8 BV510 1:200 BD Biosciences 563250
CD14 Spectral Human Mouse M5E2 BV510 1:200 BD Biosciences 740163
EpCAM Spectral Human Mouse EBA-1 BV510 1:200 BD Biosciences 563181
CD11b Spectral Human Mouse D12 BV510 1:1000 BD Biosciences 742638
CD15 Spectral Human Mouse W6D3 BV510 1:400 BD Biosciences 563141
CD45RA Spectral Human Mouse HI100 BV570 1:400 Biolegend 304131
CD244 Spectral Human Mouse C1.7 BV605 1:100 Biolegend 329536
T-BET Spectral Human Mouse O4-46 BV650 1:1000 BD Biosciences 564142
TIM3 Spectral Human Mouse 7D3 BV711 1:400 BD Biosciences 565567
CD39 Spectral Human Mouse TU66 BV750 1:400 BD Biosciences 747079
TOX Spectral Human Human cell line REA473 PE 1:800 Miltenyi 130-120-716
CTLA4 Spectral Human Mouse BNI3 PE-Cy5 1:400 BD Biosciences 555854
KLRG1 Spectral Human Syrian Hamster
2F1/KLRG1 PE-Cy7 1:400 Biolegend 138416
FOXP3 Spectral Human Mouse 236A/E7 BB700 1:20 BD Biosciences 566526
CD4 Spectral Human Mouse S3.5 Qdot800 1:100 FisherScientific 13496436
CD8 Spectral Human Mouse SK1 Spark blue 550 1:800 Biolegend 344760
CCR7 Spectral Human Mouse G043H7 Spark yg 581 1:50 Biolegend 353265
HLA-DR Spectral Human Mouse L243 Spark Violet 538 1:200 Biolegend 307678
EGFRvIII detection Spectral Human N/A N/A Biotinylated EGFRvIII peptide 1:100 FisherScientific 15876627
Streptavidin Spectral Human N/A N/A BV421 1:100 Biolegend 405226

Validation

CD45 Spectral Human Mouse HI30 AF532 1:100 FisherScientific 15560387
CD69 Spectral Human Mouse FN50 eFluor 450 1:200 FisherScientific 15568573
TCF1 Spectral Human Rabbit C63D9 AF647 1:400 Cell Signaling 6709S
LAG3 Spectral Human Mouse 3DS223H AF660 1:100 FisherScientific 17166228
KI67 Spectral Human Mouse B56 AF700 1:50 BD Biosciences 561277
CD27 Spectral Human Mouse QA17A18 APC Fire 810 1:400 Biolegend 393213
4-1BB Spectral Human Mouse 4B4 (4B4-1) APC efluor 780 1:800 FisherScientific 17123913
CD38 Spectral Human Mouse HIT2 BB515 1:200 BD Biosciences 564499
Tigit Spectral Human Mouse MBSA43 PerCP Efluor710 1:50 FisherScientific 15549426

CD28 Spectral Human Mouse CD28.2 BUV395 1:50 BD Biosciences 740308
CXCR5 Spectral Human Rat LOU RF8B2 BUV563 1:800 BD Biosciences 741316
CD25 Spectral Human Mouse 2A3 BUV615 1:200 BD Biosciences 612996
CD226 Spectral Human Mouse DX11 BUV661 1:400 BD Biosciences 749934
PD-1 Spectral Human Mouse EH12.1 BUV737 1:100 BD Biosciences 612792
CD3 Spectral Human Mouse HIT3a BUV805 1:200 BD Biosciences 741999
EOMES Spectral Human Mouse WD1928 PE-eFluor610 1:50 FisherScientific 15500517
CD127 Spectral Human Mouse HIL-7R-M21 BV480 1:50 BD Biosciences 566158
CD19 Spectral Human Mouse SJ25C1 BV510 1:200 BD Biosciences 562947
LIVE/DEAD Blue Spectral N/A N/A N/A N/A 1:1000 BD Biosciences 564406
CD41a Spectral Human Mouse HIP8 BV510 1:200 BD Biosciences 563250
CD14 Spectral Human Mouse M5E2 BV510 1:200 BD Biosciences 740163
EpCAM Spectral Human Mouse EBA-1 BV510 1:200 BD Biosciences 563181
CD11b Spectral Human Mouse D12 BV510 1:1000 BD Biosciences 742638
CD15 Spectral Human Mouse W6D3 BV510 1:400 BD Biosciences 563141
CD45RA Spectral Human Mouse HI100 BV570 1:400 Biolegend 304131
CD244 Spectral Human Mouse C1.7 BV605 1:100 Biolegend 329536
T-BET Spectral Human Mouse O4-46 BV650 1:1000 BD Biosciences 564142
TIM3 Spectral Human Mouse 7D3 BV711 1:400 BD Biosciences 565567
CD39 Spectral Human Mouse TU66 BV750 1:400 BD Biosciences 747079
TOX Spectral Human Human cell line REA473 PE 1:800 Miltenyi 130-120-716
CTLA4 Spectral Human Mouse BNI3 PE-Cy5 1:400 BD Biosciences 555854
KLRG1 Spectral Human Syrian Hamster
2F1/KLRG1 PE-Cy7 1:400 Biolegend 138416
FOXP3 Spectral Human Mouse 236A/E7 BB700 1:20 BD Biosciences 566526
CD4 Spectral Human Mouse S3.5 Qdot800 1:100 FisherScientific 13496436
CD8 Spectral Human Mouse SK1 Spark blue 550 1:800 Biolegend 344760
CCR7 Spectral Human Mouse G043H7 Spark yg 581 1:50 Biolegend 353265
HLA-DR Spectral Human Mouse L243 Spark Violet 538 1:200 Biolegend 307678
EGFRvIII detection Spectral Human N/A N/A Biotinylated EGFRvIII peptide 1:100 FisherScientific 15876627
Streptavidin Spectral Human N/A N/A BV421 1:100 Biolegend 405226

Clinical data

Policy information about clinical studies

All manuscripts should comply with the ICMJE guidelines for publication of clinical research and a completed CONSORT checklist must be included with all submissions.

Clinical trial registration	NCT03726515
Study protocol	The full study protocol is provided as an attachment.
Data collection	Data was collected at the University of Pennsylvania (Philadelphia, PA) from January, 2019 through June, 2020
Outcomes	This study's pre-specified primary endpoint was the safety and tolerability of using multiple CART-EGFRvIII (autologous T cells transduced with a lentiviral vector to express a chimeric antigen receptor specific for EGFRvIII) in combination with pembrolizumab (anti-PD-1 monoclonal antibody) for the treatment of EGFRvIII+, MGMT-unmethylated glioblastoma. Safety was evaluated based on the occurrence of study-related adverse events, using NCI CTCAE version 5.0, that occurred during the adverse event reporting period and that were determined to be related to the CART-EGFRvIII T-cell infusion, pembrolizumab, or the combination thereof. This included infusional toxicities, and any toxicity at least possibly related to these agents. Pre-specified secondary endpoints included progression-free survival and overall survival. Exploratory/correlative endpoints included measurement of CART-EGFRvIII cells in peripheral blood and tumor tissue as well as assessment of the tumor microenvironment pre vs.post-CAR T cell therapy.

Plants

Seed stocks	*Report on the source of all seed stocks or other plant material used. If applicable, state the seed stock centre and catalogue number. If plant specimens were collected from the field, describe the collection location, date and sampling procedures.*
Novel plant genotypes	*Describe the methods by which all novel plant genotypes were produced. This includes those generated by transgenic approaches, gene editing, chemical/radiation-based mutagenesis and hybridization. For transgenic lines, describe the transformation method, the number of independent lines analyzed and the generation upon which experiments were performed. For gene-edited lines, describe the editor used, the endogenous sequence targeted for editing, the targeting guide RNA sequence (if applicable) and how the editor was applied.*
Authentication	*Describe any authentication procedures for each seed stock used or novel genotype generated. Describe any experiments used to assess the effect of a mutation and, where applicable, how potential secondary effects (e.g. second site T-DNA insertions, mosiacism, off-target gene editing) were examined.*

Flow Cytometry

Plots

Confirm that:

☒ The axis labels state the marker and fluorochrome used (e.g. CD4-FITC).

☒ The axis scales are clearly visible. Include numbers along axes only for bottom left plot of group (a 'group' is an analysis of identical markers).

☒ All plots are contour plots with outliers or pseudocolor plots.

☒ A numerical value for number of cells or percentage (with statistics) is provided.

Methodology

Sample preparation	For quantification of %CD4+CAR+PD1+ cell populations: cryopreserved CAR-EGFRvIII infusion products and matched apheresis materials were thawed in complete RPMI media (RPMI 1640 supplemented with 10% FCS, 100 U/mL penicillin, 100 mg/mL streptomycin sulfate), and 0.5 U/mL benzonase (MilliporeSigma), followed by incubation at 37°C in a 5% CO2 incubator for 30 minutes. Cells were then washed with complete media without Benzonase and plated on V bottom 96-well plate. After plating, the cells were washed with PBS, stained with LIVE/DEAD Fixable Aqua (Thermo Fisher Scientific), and washed with flow buffer (PBS containing 1% BSA and 0.1% sodium azide). The cells were subsequently incubated with a surface antibodies (Abs) master mix for 20 minutes at room temperature, followed by 2 washes with flow buffer. The cells were fixed with Cytofix/Cytoperm reagents (BD Biosciences) according to the manufacturer's instructions. Following fixation, the cells were washed twice in 1× Perm/Wash Buffer and stained with Abs against an intracellular Abs master mix for 20 minutes at room temperature. The cells were finally resuspended in PBS for acquisition. For spectral cytometry: In Figure 4B, 0.5 million cells from dissociated tumor samples (see Brain Tumor Dissociation paragraph in Methods for more details) before and after CD45 magnetic beads enrichment (see Single cell RNAseq and TCRseq paragraph in Methods for more details) were stained with an anti-CD45 antibody (See Supplementary Table 2 for the antibody references). In Extended Figure 1, 0.5 million cells from the infusion products were stained with an antibody cocktail (see Supplementary Table 2 for the antibody references). See Spectral cytometry paragraph in Methods for more details on the staining.
Instrument	For quantification of %CD4+CAR+PD1+ cell populations: Cytek Aurora flow cytometer, no model number. For spectral cytometry: CyTek spectral cytometer (Aurora 4L Cell Analyzer V4)
Software	For quantification of %CD4+CAR+PD1+ cell populations: Flowjo 10.9.0 on a Mac OS X was used to perform analysis. For spectral cytometry: Omiq (https://www.omiq.ai/) was used for analyzing the data.
Cell population abundance	For quantification of %CD4+CAR+PD1+ cell populations: Relevant cell populations are listed in the Master Supplementary Tables for the relevant figures and in Extended Data Figure 4. For spectral cytometry, details are provided in the Single cell RNAseq and TCRseq paragraph in Methods section. In brief, we enriched CD45 with magnetic beads before scRNAseq and TCRseq. The proportion of CD45+ cells was 1.8% +/- 2.9% before enrichment, and we obtained an average of 41.9% +/- 23.4% CD45+ cells after enrichment.
Gating strategy	Gating strategy is described in Extended Data Figure 4. For spectral cytometry, positive and negative gates were defined using FMOs.

☒ Tick this box to confirm that a figure exemplifying the gating strategy is provided in the Supplementary Information.

Magnetic resonance imaging

Experimental design

Design type	MRI brain with and without gadolonium-based contrast was obtained per standard of care to monitor disease during the course of this clinical trial. MRIs were obtained at least every 8 weeks, or more frequently as clinically indicated.
Design specifications	*Specify the number of blocks, trials or experimental units per session and/or subject, and specify the length of each trial or block (if trials are blocked) and interval between trials.*
Behavioral performance measures	*State number and/or type of variables recorded (e.g. correct button press, response time) and what statistics were used to establish that the subjects were performing the task as expected (e.g. mean, range, and/or standard deviation across subjects).*

Acquisition

Imaging type(s): structural, diffusion, perfusion

Field strength: 3T

Sequence & imaging parameters: Imaging protocol included axial T1-weighted 3D MPRAGE before and after contrast, post-contrast axial FLAIR, dynamic contrast-enhanced (DCE) perfusion, and dynamic susceptibility contrast (DSC) perfusion.

Area of acquisition: Whole brain scan

Diffusion MRI ☐ Used ☒ Not used

Preprocessing

Preprocessing software: *Provide detail on software version and revision number and on specific parameters (model/functions, brain extraction, segmentation, smoothing kernel size, etc.).*

Normalization: *If data were normalized/standardized, describe the approach(es): specify linear or non-linear and define image types used for transformation OR indicate that data were not normalized and explain rationale for lack of normalization.*

Normalization template: *Describe the template used for normalization/transformation, specifying subject space or group standardized space (e.g. original Talairach, MNI305, ICBM152) OR indicate that the data were not normalized.*

Noise and artifact removal: *Describe your procedure(s) for artifact and structured noise removal, specifying motion parameters, tissue signals and physiological signals (heart rate, respiration).*

Volume censoring: *Define your software and/or method and criteria for volume censoring, and state the extent of such censoring.*

Statistical modeling & inference

Model type and settings: *Specify type (mass univariate, multivariate, RSA, predictive, etc.) and describe essential details of the model at the first and second levels (e.g. fixed, random or mixed effects; drift or auto-correlation).*

Effect(s) tested: *Define precise effect in terms of the task or stimulus conditions instead of psychological concepts and indicate whether ANOVA or factorial designs were used.*

Specify type of analysis: ☒ Whole brain ☐ ROI-based ☐ Both

Statistic type for inference: *Specify voxel-wise or cluster-wise and report all relevant parameters for cluster-wise methods.*

(See Eklund et al. 2016)

Correction: *Describe the type of correction and how it is obtained for multiple comparisons (e.g. FWE, FDR, permutation or Monte Carlo).*

Models & analysis

n/a	Involved in the study
☒	☐ Functional and/or effective connectivity
☒	☐ Graph analysis
☒	☐ Multivariate modeling or predictive analysis